USGS
science for a changing world

# Geologic Map of the Ariel Quadrangle, Clark and Cowlitz Counties, Washington

By Russell C. Evarts

Pamphlet to accompany
Scientific Investigations Map 2826

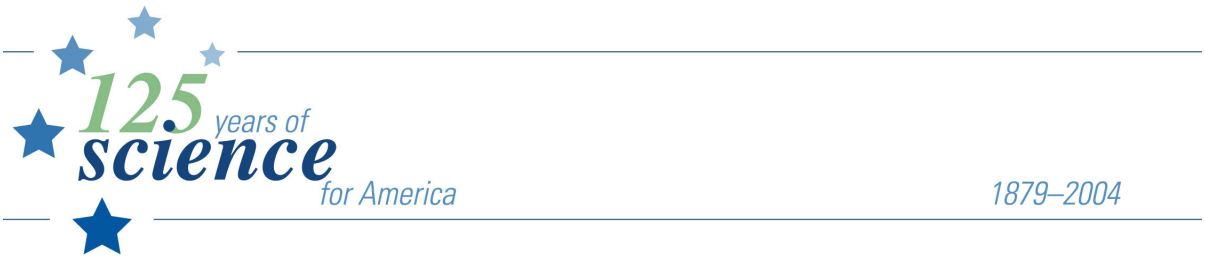


2004

U.S. Department of the Interior
U.S. Geological Survey

# INTRODUCTION

## GEOGRAPHIC AND GEOLOGIC SETTING

The Ariel 7.5' quadrangle is situated along the Puget-Willamette Lowland approximately 50 km north of Portland, Oregon (fig. 1). The lowland, which extends from Puget Sound into west-central Oregon, is a complex structural and topographic trough that lies between the Coast Range and the Cascade Range. Since late Eocene time, the Cascade Range has been the locus of an active volcanic arc associated with underthrusting of oceanic lithosphere beneath the North American continent along the Cascadia Subduction Zone. The Coast Range occupies the forearc position within the Cascadia arc-trench system and consists of a complex assemblage of Eocene to Miocene volcanic and marine sedimentary rocks.

The Ariel quadrangle lies along the northeastern margin of the Portland Basin, a roughly 2000-km$^2$ topographic and structural depression in the central Puget-Willamette Lowland (Beeson and others, 1989; Swanson and others, 1993; Yeats and others, 1996). The Portland Basin is approximately 70 km long and 30 km wide; its long dimension is oriented northwest. Its northern boundary coincides, in part, with the lower Lewis River, which flows southwestward through the map area. The Lewis drains a large area in the southern Washington Cascade Range, including the southern flank of Mount St. Helens approximately 25 km upstream from the quadrangle, and joins the Columbia River about 12 km west of the quadrangle (fig. 1). The flanks of the Portland Basin consist of deformed and eroded Eocene through Miocene volcanic and sedimentary rocks that rise to elevations exceeding 2000 ft (610 m). Seismic-reflection profiles (L.M. Liberty, written commun., 2003) and lithologic logs of water wells (Swanson and others, 1993; Mabey and Madin, 1995) indicate that as much as 550 m of late Miocene and younger sediments have accumulated in the deepest part of the basin near Vancouver. Most of this basin-fill material was carried in from the east by the Columbia River, but sediment deposited by streams draining the adjacent highlands is locally important.

The Portland Basin has been interpreted as a pull-apart basin located in the releasing stepover between two en echelon, northwest-striking, right-lateral fault zones (Beeson and others, 1985, 1989; Beeson and Tolan, 1990; Yelin and Patton, 1991; Blakely and others, 1995). These fault zones are thought to reflect regional transpression and dextral shear within the forearc in response to oblique subduction of the Pacific Plate along the Cascadia Subduction Zone (Pezzopane and Weldon, 1993; Wells and others, 1998). The southwestern margin of the Portland Basin is a well-defined topographic break along the base of the Tualatin Mountains, an asymmetric anticlinal ridge that is bounded on its northeast flank by the Portland Hills Fault Zone (Balsillie and Benson, 1971; Beeson and others, 1989; Blakely and others, 1995), which is probably an active structure (Wong and others, 2001; Liberty and others, 2003). The nature of the corresponding northeastern margin of the basin is less clear, but a poorly defined and partially buried dextral extensional fault zone has been hypothesized from topography, microseismicity, potential field-anomalies, and reconnaissance geologic mapping (Beeson and others, 1989; Beeson and Tolan, 1990; Yelin and Patton, 1991; Blakely and others, 1995).

This map is a contribution to a program designed to improve the geologic database for the Portland Basin region of the Pacific Northwest urban corridor, the densely populated Cascadia forearc region of western Washington and Oregon. Better and more detailed information on the bedrock and surficial geology of the basin and its surrounding area is needed to refine assessments of seismic risk (Yelin and Patton, 1991; Bott and Wong, 1993), ground-failure hazards (Madin and Wang, 1999; Wegmann and Walsh, 2001) and resource availability in this rapidly growing region. The digital database for this publication is available on the World Wide Web at http://pubs.usgs.gov/sim/2004/2826.

## PREVIOUS GEOLOGIC INVESTIGATIONS

Previous geologic mapping in the Ariel quadrangle, generally carried out as part of broad regional reconnaissance investigations, established the basic stratigraphic framework and distribution of geologic units in the quadrangle. The first systematic geologic investigation within the Ariel quadrangle was that of Mundorff (1964), who mapped the area south of the Lewis River to evaluate water resources in Clark County. His 1:48:000-scale map accurately portrays contacts between Tertiary bedrock and the basin-fill units, although he made no attempt to map stratigraphic units within the Tertiary sequence. He proposed a two-fold division of the Troutdale Formation into a lower fine-grained member and an upper coarse-grained member, but did not show the distribution of these members on his map. Mundorff (1964, 1984) described Pleistocene drift and glacier-outburst flood deposits in the

Lewis River system but did not distinguish deposits derived from the Quaternary volcanic center of Mount St. Helens.

Swanson and others (1993) updated Mundorff's Clark County work as part of an investigation of ground-water resources throughout the Portland Basin. Their work focused on the basin-fill units, and their map shows hydrogeologic rather than stratigraphic units, although there is substantial equivalence between the two. For example, they showed the distribution of a fine-grained confining unit that corresponds to Mundorff's lower member of the Troutdale Formation. They analyzed lithologic logs of 1500 water wells to produce a series of maps showing the elevations and thicknesses of the hydrogeologic units throughout the basin, thus constructing a rough 3-dimensional view of the subsurface stratigraphy of the basin fill.

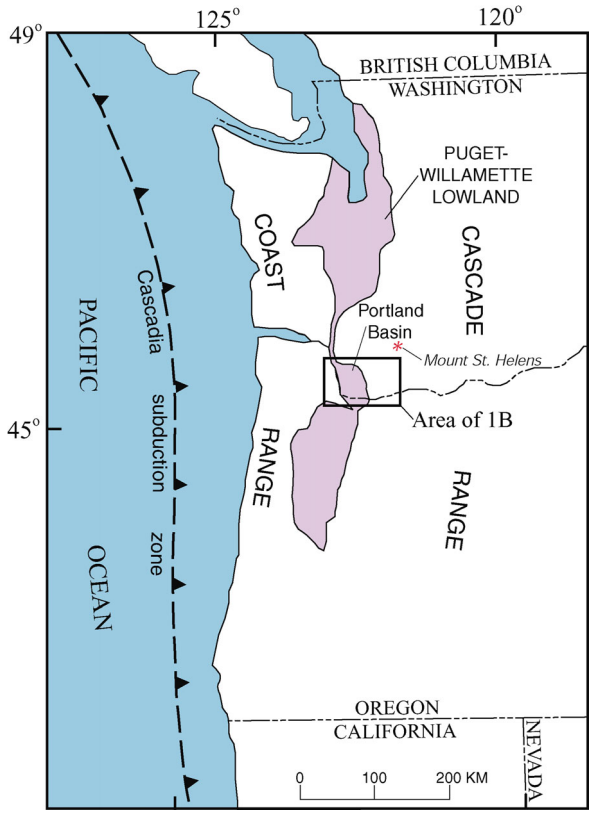


**Figure 1A.** Regional setting of the Ariel quadrangle showing major tectonic and physiographic features of the Pacific Northwest.

Phillips (1987a) compiled a geologic map of the Vancouver 30' x 60' quadrangle, which includes the Ariel 7.5' quadrangle, at 1:100,000 scale as part of the state geologic map program of the Washington Division of Geology and Earth Resources (Walsh and others, 1987). Although relying heavily on Mundorff's work, he did undertake some original reconnaissance mapping. Phillips was the first to depict the Mount St. Helens-derived deposits in the lower Lewis River valley. He also mapped informal lithostratigraphic units within the Tertiary bedrock sequence. He acquired chemical analyses for some of the volcanic rocks of the region as well as a few whole-rock K-Ar age determinations, although none of these new data were obtained from the Ariel quadrangle.

Some topical investigations have provided additional information on the geology of the Ariel quadrangle and vicinity. Detailed geologic mapping and drilling was conducted during construction of Merwin Dam (Williams, 1933; I.A. Williams, unpublished report, 1930, summarized in Tilford and Sullivan, 1981, and Bliton, 1989). Mundorff (1984) followed up his Clark County hydrogeologic investigation with a report on glacial deposits of the Lewis River region. Major and Scott (1988) studied the Mount St. Helens-related deposits of the Lewis River valley, which they described but did not map. Cores obtained from deposits at Fargher Lake have been used in

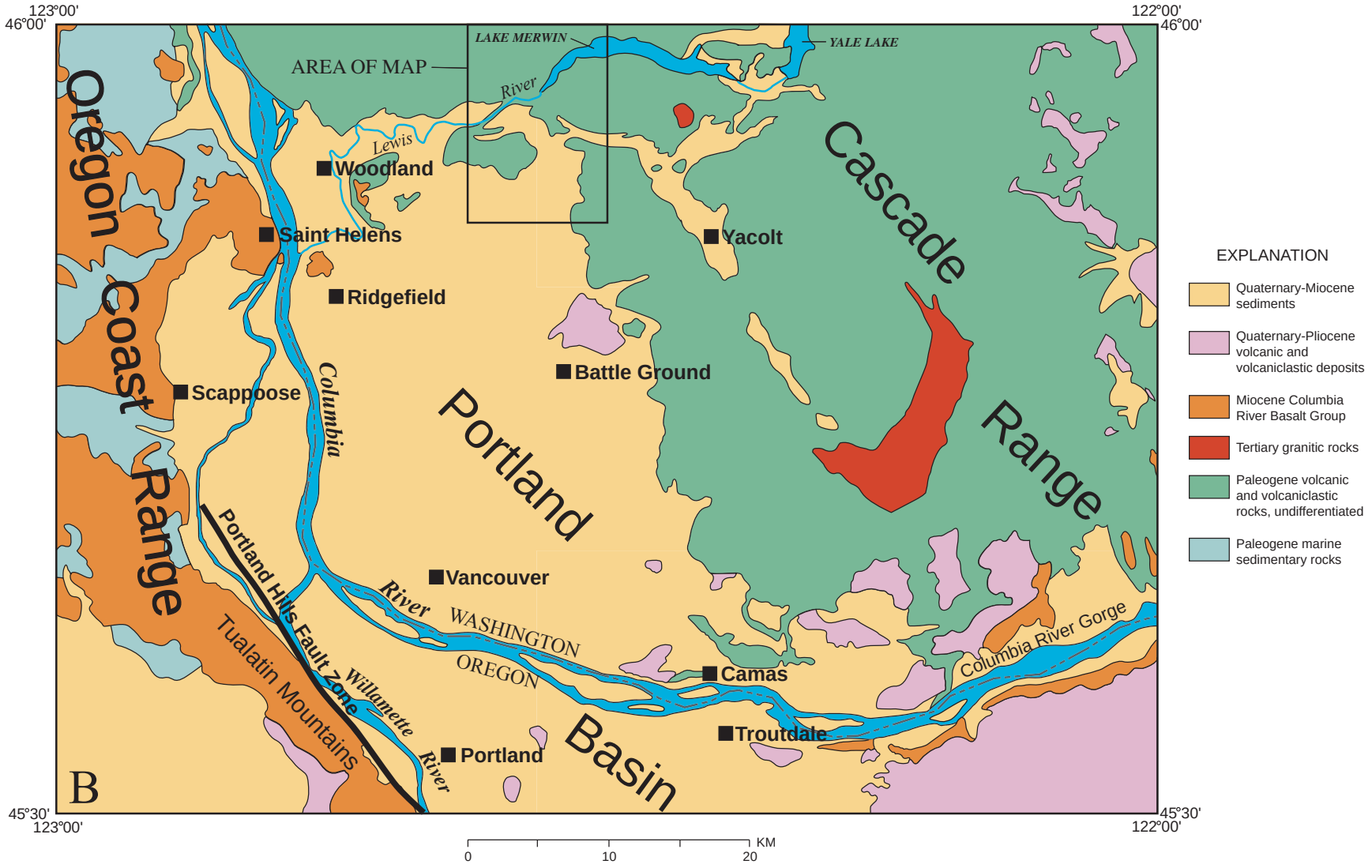


**Figure 1B.** Simplified geologic map of the Vancouver 30' x 60' quadrangle, modified from Phillips (1987a).

several studies of late Quaternary climatic variations and paleomagnetic variations (Heusser and Heusser, 1980; Barnosky, 1984; Doh and Steele, 1983; Grigg and Whitlock, 2002). Fiksdal (1975) mapped landslides and delineated areas of potential slope instability in Clark County.

ACKNOWLEDGMENTS

Access granted by landowners was essential for mapping in the Ariel quadrangle. I thank Robert Ross and Dennis Mohan of the Longview Fibre Company, Ross Graham and Dorothy Yount of Weyerhaeuser Company, and Ann Wikman of the Southwest Regional Office of the Washington Division of Natural Resources for permission to work on their timberlands. Anna King, Richard Barney, and William Fields of PacifiCorp permitted work on the lands adjacent to Lake Merwin. Several U.S. Geological Survey colleagues provided data: David Siems (analytical chemistry), Richard Blakely (aeromagnetic maps), Andrei Sarna-Wojcicki (tephrochronology), and Robert Fleck ($^{40}Ar/^{39}Ar$ ages). Chemical analyses at Washington State University were performed by Diane M. Johnson. Kevin Anderson, Bradley Reid, and Christopher DuRoss gave able field and laboratory assistance. Sarna-Wojcicki, Kenneth Bishop, Judith Fierstein, and Michael Clynne made available essential laboratory facilities. Debra Hunemuller, Stephanie Abraham, and Tammy Howes of the Washington Department of Ecology Southwest Regional Office in Lacey, Washington provided access to files of water-well drillers' logs. Connie Manson helped obtain unpublished information from the library at the Washington Division of Geology and Earth Resources in Olympia, Washington. I have benefited immensely from discussions on various aspects of the regional stratigraphy, structure, and geologic history of southwestern Washington with Roger Ashley, Michael Clynne, Paul Hammond, Keith Howard, Alan Niem, Jim O'Connor, William Phillips, William Scott, James Smith, Donald Swanson, Karl Wegmann, and Ray Wells. Field and office consultations with Scott and Clynne helped greatly with the identification and interpretation of Mount St. Helens-derived deposits; Clynne also provided chemical analyses of four Mount St. Helens dacites that are included in table 1. Keith Howard and Edwin McKee provided valuable technical reviews.

## SYNOPSIS OF GEOLOGY

The geology of the Ariel quadrangle is dominated by three major groups of deposits: Paleogene bedrock, late Miocene and Pliocene(?) alluvial deposits of the ancestral Columbia River, and Quaternary alluvial and glaciofluvial deposits in the Lewis River valley. Bedrock underlies the dissected upland north of the Lewis River and is exposed at places beneath younger deposits south of the river. It consists of a diverse assemblage of late Eocene and earliest Oligocene volcanic and volcaniclastic rocks and small intrusions, which are early products of the Cascade volcanic arc. Following mild folding, faulting, and erosion, the bedrock units formed a low-relief terrain within which the Portland Basin began to develop during early Neogene time. Basaltic lavas of the Columbia River Basalt Group (not exposed in this quadrangle) and fluvial deposits of the ancestral Columbia River were deposited on the Paleogene bedrock within the subsiding basin. During Pleistocene and Holocene time, alluvial processes in the Lewis River valley have been strongly influenced by regional uplift of the Cascade Range, glaciation in the Cascade Range, eruptive activity at the Mount St. Helens volcanic center, and cataclysmic flooding triggered by the failure of ice dams at glacial Lake Missoula in Montana.

A relatively mild, wet climate prevailed in the western Pacific Northwest throughout most of the Cenozoic era (Wolfe and Hopkins, 1967; Wolfe, 1978). Mountain glaciers formed in the Lewis River valley on several occasions during the Pleistocene (Crandell and Miller, 1974; Mundorff, 1984); the largest extended downvalley into the map area and spread over the low-relief terrain to the south. Glaciation left behind a smoothed topography of bedrock hills and valleys mantled by variable thicknesses of drift. In areas beyond the reach of glacial ice, however, long exposure produced saprolitic soil horizons as much as several meters thick on Paleogene bedrock and the Troutdale Formation. This weathering can make it difficult to distinguish between sedimentary units of different ages. Because of this intense weathering and the dense vegetation of the region, natural outcrops of bedrock are generally limited to steep cliff faces, landslide scarps, and streambeds; most exposures are at roadcuts and quarries. Surface information was supplemented with lithologic data obtained from water-well reports in the files of the Washington Department of Ecology; well locations were taken as described in the reports and were not field checked.

## PALEOGENE BEDROCK

Bedrock in the Ariel quadrangle consists of a diverse assortment of subaerially erupted lava flows and volcaniclastic rocks that are typical of the strata that underlie much of the western slopes of the southern Washington Cascade Range (Evarts and others, 1987; Smith, 1993; Evarts and Swanson, 1994). Bedrock units in the quadrangle generally strike east-west to northeast and dip south to southeast at 15° to 30°. In the northwestern part of the quadrangle, this pattern is disrupted by complex structures related to development of a caldera complex. Fine- to coarse-grained mafic to silicic intrusive rocks are abundant in the vicinity of the caldera; the intrusions exhibit a pronounced N. 75° E. preferred orientation. $^{40}Ar/^{39}Ar$ age determinations (R.J. Fleck, written commun., 2000, 2001, 2003) obtained for bedrock units within this and adjacent quadrangles indicate that the extrusive and sedimentary rocks in the map area are mostly between 37 and 34 millions years old, that is, late Eocene, but those in the southeasternmost part of the map area may be earliest Oligocene. Ages of the intrusions are unknown but most are believed to be no more than a few million years younger than their host rocks.

### STRATIGRAPHIC NOMENCLATURE: THE GOBLE PROBLEM

Phillips (1987a) assigned most of the Eocene rocks of the Ariel quadrangle to the Goble Volcanics. The Goble Volcanic Series was named by Wilkinson and others (1946) for volcanic and volcaniclastic rocks exposed along the Columbia River near Goble, Oregon, about 20 km west of the map area. The name was later revised to Goble Volcanics by Livingston, 1966, to conform to the then-current North American Code of Stratigraphic Nomenclature. Wilkinson and others (1946) stated that the formation "extends eastward . . . to the Lake Merwin area". As discussed by Evarts (2002), the difficulty with employing the Goble Formation as a formal stratigraphic unit in Washington is that the Oligocene marine sedimentary unit that defines the top of the formation in Oregon does not extend into Washington. Instead, the rocks mapped as Goble by Wilkinson and others (1946) east of the Columbia River constitute only the lower part of a thick pile of Paleogene to early Neogene volcanic rocks that underlie most of the western slope of the southern Washington Cascade Range (see Evarts and Swanson, 1994, and references therein). This heterogeneous sequence includes many flows and volcaniclastic beds lithologically indistinguishable from the rocks exposed near Goble, and no pronounced lithologic break correlative with the top of the Goble Volcanics in Oregon is apparent in Washington. Phillips (1987a, b, written commun., 1986) suggested that the Goble Volcanics of Wilkinson and others (1946) was overlain in Washington by a regionally persistent horizon of volcaniclastic rocks (his unit $Tvc_1$) that separated the Goble Volcanics from overlying Oligocene volcanic rocks. However, detailed mapping in this and adjoining areas (Evarts and Ashley, 1990a, b, 1991, 1992; Evarts, 2002, 2004; R.C. Evarts, unpub. mapping) shows that stratigraphic relations are more complex than portrayed by Phillips, and the volcaniclastic unit he mapped actually represents several stratigraphic levels. In the absence of a clear lithologic break to mark the upper contact of the Goble Volcanics, the name is not employed here, and only informal or lithologic names are used for the volcanic rocks shown on this map.

### VOLCANIC AND VOLCANICLASTIC ROCKS

#### Basaltic andesite, andesite, and basalt

Mafic to intermediate lava flows and flow breccia are major components of the Paleogene section of the Ariel quadrangle. Basaltic andesites (Tba) range from seriate to conspicuously porphyritic, with phenocrysts of plagioclase, olivine, and augite. A sequence of basaltic andesite flows distinguished by the presence of hypersthene phenocrysts (Thba), crops out in the northwestern part of the quadrangle. The basaltic andesites typically form blocky to platy jointed flows 3 to 6 m thick that grade into upper and lower flow breccia zones. Upper flow breccia zones are characterized by abundant zeolite- and clay-filled vesicles and reddish colors owing to oxidation during cooling. All flows were apparently emplaced subaerially; no pillow lavas or other indications of subaqueous environments were observed. Andesitic lava flows and flow breccias (Ta) exhibit a range of textures from aphyric to moderately porphyritic; all porphyritic flows are pyroxene andesites that contain phenocrysts of augite, hypersthene, or both.

Basalt flows are uncommon in the Ariel quadrangle. Two types have been distinguished based on the presence or absence of feldspar phenocrysts. Two isolated flows of olivine+plagioclase-phyric basalt (Tb) crop out peripheral to the Davis Peak caldera, one in upper Colvin Creek drainage and one near the drainage divide

separating Cape Horn and Marble Creeks. One or more flows of distinctive feldspar-free olivine-phyric basalt (Tob) are present between Cedar Creek and Bald Mountain. The olivine phenocrysts in the flows contain abundant euhedral inclusions of chromian spinel and, unlike those in other mafic rocks, are not completely altered. Petrographically similar olivine-phyric flows were mapped by Evarts (2004) in the Woodland quadrangle to the west and by Evarts and Ashley (1991) in the Lakeview Peak quadrangle to the northeast, but they appear to be older than the basalt flows in the Ariel quadrangle.

### Dacite and rhyolite

The largest accumulations of silicic volcanic rocks in the Ariel quadrangle are designated the dacite of Marble Creek (Tdm) and the rhyolite of Bald Mountain (Trb). The dacite of Marble Creek is a pile of platy dacite flows and breccia, 500 m or more thick, that underlies much of the drainage divide between Cape Horn Creek and the Lewis River. The unit thins markedly away from this area and is less than 100 m thick southeast of Lake Merwin. It is interpreted as a flow-dome complex. The rocks are moderately porphyritic and universally altered to argillic or propylitic mineral assemblages. The dacite of Marble Creek is truncated to the west by the steep margin of the Davis Peak caldera. It is among the youngest pre-caldera stratigraphic units and may represent immediately precursor silicic volcanism. As much as 200 m of porphyritic hypersthene rhyolite underlies Bald Mountain. Most samples of this low-silica rhyolite exhibit extensive alteration to clay minerals; plagioclase is kaolinitized and hypersthene phenocrysts are replaced by smectite. Unlike the older dacite of Marble Creek, this unit lacks internal flow contacts and breccias and most likely is an exhumed plug dome.

Isolated silicic flows (Td and Tr) are dispersed throughout all but the lowest part of the Paleogene stratigraphic section of the Ariel quadrangle. Textures range from distinctly porphyritic to nearly aphyric. Some of these flows exhibit pronounced, locally contorted, flow banding.

### Volcaniclastic rocks

Volcaniclastic rocks make up a substantial proportion of the Paleogene bedrock in the Ariel quadrangle and are divided into: (1) a unit of volcaniclastic sedimentary rocks of predominantly epiclastic origin (Tvs); (2) a tuff unit comprised of mostly pyroclastic rocks (Tt); and (3) a complex assemblage of tuff and breccia associated with formation of the Davis Peak caldera (Tdpc and Tdpo) that is discussed separately below.

Volcaniclastic sedimentary rocks (Tvs) constitute a diverse assemblage of generally well bedded, texturally and compositionally immature siltstone, sandstone, conglomerate, and breccia. Fragments of volcanic rocks petrographically similar to interbedded lava flows are the dominant constituents of most beds; less abundant components include plagioclase, Fe-Ti oxides, and pyroxene crystals, pumice, vitric ash, fine-grained dioritic rocks, and plant remains. Strata of the volcaniclastic sedimentary rocks unit (Tvs) represent a variety of depositional environments and include thin debris-flow and hyperconcentrated flood-flow (Smith, 1986) deposits as well as finer grained fluvial and lacustrine beds probably deposited beyond the flanks of volcanic edifices. In addition to material eroded from older extrusive rocks, many beds likely contain clasts reworked from unconsolidated penecontemporaneous airfall and ash-flow deposits.

The tuff unit (Tt) consists of andesitic to rhyolitic tuff, pumiceous and lithic lapilli tuff, and lithic tuff breccia that are inferred to be the direct products of explosive eruptions and volcanic debris flows. Massive, medium- to coarse-grained, poorly sorted, and matrix-supported beds typify this unit. Beds that contain abundant pumice lapilli, originally vitric ash, and carbonized woody debris are interpreted as ignimbrites. Phenocrysts rarely constitute more than 10 percent of juvenile material in these tuff beds, and include plagioclase, augite, hypersthene, and Fe-Ti oxide, but no quartz, hornblende or biotite. The unit also includes diamictites of inferred lahar or block-and-ash-flow origin that contain angular clasts of volcanic rock as large as 5 m across in a tuffaceous matrix; such beds are well exposed in Cedar Creek 0.8 km east-southeast of Etna and on the east bank of the Lewis River directly below Merwin Dam.

### Davis Peak caldera

A thick and stratigraphically complex section of tuff and breccia south of Davis Peak (Tdpc) is interpreted as fill in a roughly circular caldera about 3.5 km in diameter. The caldera probably formed by foundering of a stratovolcano complex following partial evacuation of an underlying magma chamber as a result of a massive pyroclastic eruption, analogous to the collapse of Holocene Mount Mazama in Oregon to produce Crater Lake

caldera (Bacon, 1983). At least 500 m of caldera-fill deposits are exposed in steep tributaries of Johnson, Colvin, Husky, and Cape Horn Creeks. The predominant component of these intracaldera deposits is densely welded, porphyritic, pumiceous lapilli tuff of dacitic composition, which contains variable proportions of lithic volcanic clasts. Complexly interdigitated with the tuff is coarse diamictite that is interpreted as landslide breccia generated by syneruptive caving of oversteepened caldera walls, similar to that described by Lipman (1997). In some areas, such as upper Husky Creek, diamictite makes up most of the caldera fill. Also present are more-or-less coherent megablocks tens of meters across of lava encased within lapilli tuff; these are probably fragments of the collapsed roof of the magma chamber. Much of the intracaldera fill is devitrified or propylitized. The ridge extending south from Davis Peak near the top of the fill, however, is underlain by densely welded vitrophyre. An aeromagnetic map of the Ariel quadrangle (R.J. Blakely, written commun., 1999) shows a pronounced positive anomaly about 1 km across that lies directly beneath the ridge; this anomaly may reflect a shallow subsided block of precaldera basaltic andesite. Such a block could have shielded the overlying tuff from ascending hydrothermal fluids and thus inhibited devitrification. The vitrophyre contains abundant phenocrysts of plagioclase, lesser amounts of augite and hypersthene, and sparse lithic fragments in a matrix of orange hydrated glass. An $^{40}Ar/^{39}Ar$ age of 35.2±0.3 Ma was obtained from the plagioclase (table 2).

The structural margin of the caldera is a subvertical ring fault locally intruded by diorite. It approximately coincides with a moat-like magnetic low (R.J. Blakely, written commun., 1999). Within the area bounded by the fault, structural attitudes defined by fiamme are commonly steep and tend to dip radially inward, in marked contrast to the low to moderate south to southeast dips that typify the regional structural trend. Locally, compaction foliation varies widely in orientation over short distances, especially in the vicinity of megablocks. As mapped, the ring fault encloses several large coherent blocks more than a kilometer across. The rocks of these blocks are similar to pre-caldera strata but locally display pervasive fine-scale fracturing and exhibit structural attitudes discordant to the regional trend. The best example is the triangular (in plan view) block of north-dipping strata along the southern margin of the caldera. These huge blocks appear to have been rotated but not transported laterally. Intracaldera tuff appears to be banked against steep block-bounding faults, creating buttress unconformities. The blocks are interpreted as fragments of the original roof of the subcaldera magma chamber that subsided chaotically during the paroxysmal eruption to form a fragmented caldera floor, similar to the piecemeal calderas described by Branny and Kokelaar (1994) and Branney (1995). The deep erosional level implied by the exposure of the floor is consistent with the pervasive propylitic alteration and abundant phaneritic intrusions (see, for example, Lipman, 1984).

A bed of densely welded tuff (Tdpo) that closely resembles the intracaldera tuff near Davis Peak crops out east of Bald Mountain and south of Cedar Creek. Its $^{40}Ar/^{39}Ar$ age of 35.1±0.3 Ma (table 2) is analytically indistinguishable from that of the tuff near Davis Peak. It is interpreted as a remnant of the outflow facies of the tuff of Davis Peak, emplaced by pyroclastic flows generated by the paroxysmal eruption.

## INTRUSIVE ROCKS

Intrusive rocks of mafic to silicic composition are scattered throughout the Ariel quadrangle but are far more abundant north of the Lewis River. In this area, dikes and other small intrusions are undoubtedly more common than portrayed on the map but their abundance is apparent only in a few well exposed localities such as along the bed of Cape Horn Creek.

Several composite bodies of sparsely porphyritic pyroxene dacite (Tid) are confined within the Davis Peak caldera. These intrusions may have been emplaced shortly after collapse and fed postcaldera dacite domes, as observed at some other calderas (Lipman, 1984).

Most intrusions in the Ariel quadrangle belong to a swarm of dikes, sills, and irregular bodies concentrated in a 4-km-wide belt that extends across the north half of the map area and about 7 km west into the Woodland quadrangle (Evarts, 2004). The dikes, typically 1 to 3 m wide, exhibit a strong preferential orientation: they strike N. 75° E., parallel to the overall trend of the belt, and dip about 70° N. A few larger bodies are also elongate in this N. 75° E. direction. Other intrusions were emplaced along the ring fault of the Davis Peak caldera. Many of the larger bodies are composite, comprising multiple phases of varying composition and texture. Collectively, the intrusions range from mafic to intermediate in composition and vary in texture from fine-grained rocks petrographically similar to their extrusive host rocks (Tiba, Tia) to medium- and coarse-grained gabbro (Tgb), pyroxene diorite (Tdi), and quartz diorite (Tqd). Nearly all the intrusions are deuterically altered, some intensely so. They appear to form a coherent magmatic suite.

None of the intrusions has been radiometrically dated. The coarse grain size of some of the intrusions is consistent with slow cooling at depth, which implies that crystallization occurred after their late Eocene host rocks had been buried beneath perhaps several hundred meters of younger strata. Also, the pronounced N. 75° E. strike of the dikes is superimposed on the caldera, which indicates that emplacement occurred within a regional tectonic stress regime established after cessation of late Eocene volcanic activity at the Davis Peak center. Restoration of precaldera host strata to a horizontal orientation rotates the dikes to near vertical; this suggests emplacement prior to folding, which from regional considerations probably took place in early Miocene time (Evarts and Swanson, 1994). Therefore, most intrusions probably were emplaced during Oligocene time, although some of the fine-grained dikes (Tiba, Tia, Tid) may mark subvolcanic feeders for the late Eocene extrusive rocks.

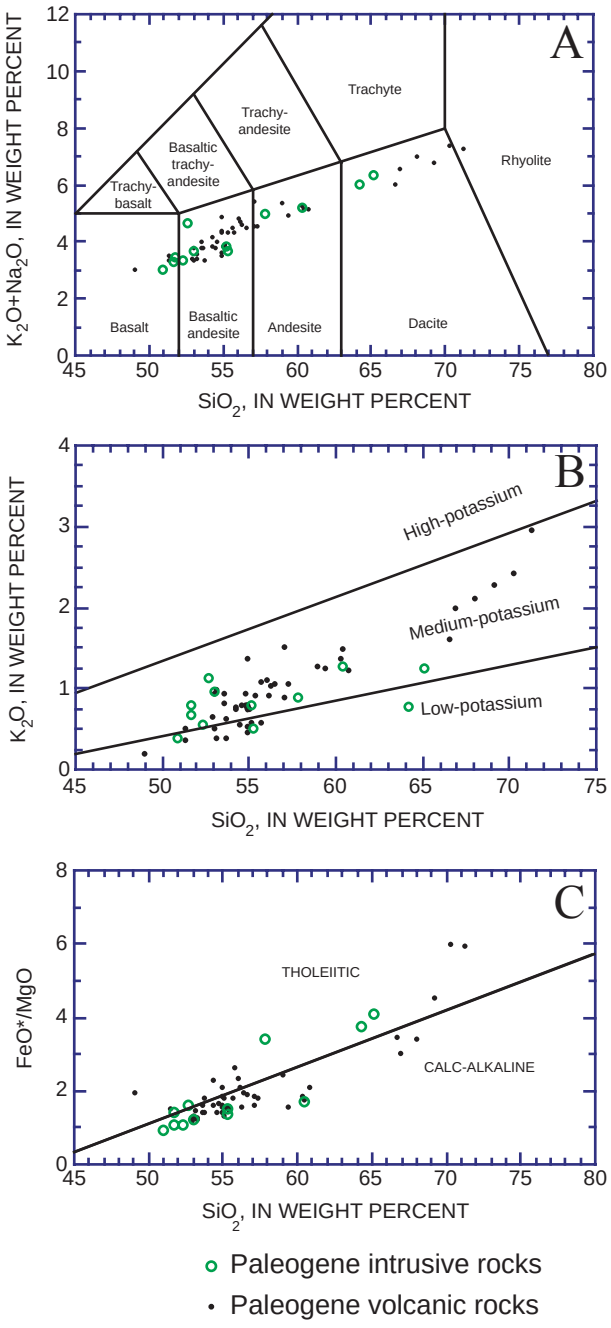


**Figure 2.** Chemical characteristics of volcanic rocks from the Ariel 7.5' quadrangle (analyses recalculated volatile-free). A, $K_2O+Na_2O$ versus $SiO_2$, showing IUGS classification (Le Maitre, 2002); B, $K_2O$ versus $SiO_2$, showing low-, medium-, and high-potassium fields extrapolated from Gill (1981, p. 6); C, FeO*/MgO versus $SiO_2$, showing classification into tholeiitic and calc-alkaline rocks according to Miyashiro (1974). FeO*, total Fe as FeO.

## ROCK CHEMISTRY

The chemistry of Paleogene lava flows and intrusive rocks in the Ariel quadrangle (table 1) generally resembles that of Tertiary igneous rocks sampled elsewhere in the southern Washington Cascade Range (Evarts and Ashley, 1990a,b, 1991, 1992; Evarts and Bishop, 1994; Evarts and Swanson, 1994; Evarts, 2001, 2002, 2004; R.C. Evarts, unpub. data). The compositions of igneous rocks in the quadrangle range from basalt to rhyolite (fig. 2A) and form a low- to medium-potassium suite (fig. 2B) that straddles the dividing line between tholeiitic and calc-alkaline compositions using the classification of Miyashiro (1974; fig. 2C). $TiO_2$ contents are low, generally less than 1.5 wt percent (table 1), as is typical for volcanic-arc magmas (Gill, 1981). No significant chemical differences between eruptive and intrusive magmas are apparent in the data.

## METAMORPHISM AND HYDROTHERMAL ALTERATION

Paleogene rocks in the Ariel quadrangle have been subjected to zeolite-facies regional metamorphism, the general character of which is similar to that described from other areas in the southern Washington Cascade Range (Fiske and others, 1963; Wise, 1970; Evarts and others, 1987; Evarts and Swanson, 1994). This region-wide

metamorphism reflects burial of the late Eocene and early Oligocene rocks by younger volcanic rocks within the relatively high-heat-flow environment of an active volcanic arc. Superimposed on the background zeolitization is an area of more intense hydrothermal alteration reflected in the development of propylitic assemblages and (or) pervasive replacement by carbonate and clay minerals. This metasomatic alteration is spatially coextensive with, and genetically related to, the concentration of intrusive bodies north of the Lewis River.

In rocks subjected to zeolite-facies metamorphism, the extent of replacement of igneous minerals by secondary phases ranges from incipient to complete. Permeable, glass-rich, silicic volcaniclastic rocks are the most susceptible to zeolitization, whereas massive lava flows may be only slightly affected. The primary effect of very-low-grade metamorphism in mafic to intermediate-composition lava flows is the development of clay minerals and zeolites that replace labile interstitial glass, fill vesicles, and are deposited on joint surfaces. Feldspar typically is partially altered to clay minerals and (or) zeolites along fractures and cleavage planes. Olivine phenocrysts in most basalts and basaltic andesites are totally replaced by smectite with or without hematite and calcite; replacement is incomplete, however, in some olivine-rich flows. Primary augite and Fe-Ti oxides are largely unaffected by the zeolite-facies metamorphism. Hypersthene phenocrysts in pyroxene andesite flows commonly exhibit minor replacement by dark brown smectite. In pervasively altered volcaniclastic rocks and flow breccias, smectitic clay minerals and zeolites pseudomorphically replace most framework grains and fill pore spaces; the development of iron-rich smectites gives these rocks their characteristic green colors. The widespread presence of heulandite and clinoptilolite in the volcaniclastic rocks of this quadrangle indicates that, except for areas near intrusions, metamorphic temperatures did not exceed 180°C (Cho and others, 1987). Originally glassy silicic flows and domes commonly exhibit pervasive devitrification and alteration to cryptocrystalline quartz, feldspar, kaolinite, calcite, zeolites, and hematite. Plagioclase phenocrysts are partly to completely replaced by albite, clay minerals, and carbonates; pyroxene phenocrysts are rarely preserved. Alteration of this type is common in Tertiary silicic lavas in the Cascade Range (Evarts and others, 1987) because the viscous flows accumulate near source vents where they are exposed to postcrystallization fumerolic activity.

Propylitic assemblages north of the Lewis River are characterized by the widespread development of epidote, albite, chlorite, pyrite, and calcite. The metamorphic minerals occur as fine-grained replacements of igneous phases, in amygdules, and as fracture fillings. This alteration increases in intensity with depth, and higher temperature metamorphism is recorded by the local occurrence of amphibole-bearing assemblages. The intrusions are commonly similarly affected, obscuring the distinction in the field between fine-grained intrusive rocks and their host rock. Metamorphic effects extend beyond the confines of the caldera and are interpreted as albite-epidote-hornfels-facies hydrothermal contact metamorphism caused by the abundant intrusions. Similar alteration is developed in the vicinity of stocks and plutons throughout the western Cascade Range (Buddington and Callaghan, 1936; Grant, 1969; Evarts and others, 1987).

Surrounding the area of propylitized rock is a broad fringe, coextensive with the dike swarm, in which secondary calcite is widely distributed as veins and replacements in the volcanic rocks. The general spatial association of carbonate with intrusive rocks suggests that the $CO_2$ was introduced by devolatilization of the intrusions. Sporadically distributed within the calcite-bearing fringe are patches of more intense metasomatic hydrothermal alteration in which primary feldspar and pyroxene minerals are partly to completely replaced by some combination of albite, calcite, chlorite, epidote, montmorillonite, kaolinite, zeolites, quartz, titanite, and pyrite. The metasomatic hydrothermal alteration is attributed to reactions with low-temperature hydrothermal fluids generated from cooling intrusions at depth and circulated widely through the upper crust along permeable structural zones; therefore, the presence of such alteration provides an important clue for inferring the existence of faults within the poorly exposed Paleogene section.

An unusual type of alteration, which is characterized by the assemblage tourmaline + sericite + quartz ± pyrite, is exposed in the headwaters of Marble Creek. Although complete reconstitution obscures the protolith, vague porphyritic textures suggest the altered rock belongs to the dacite of Marble Creek. Locally the altered rock is a coarse breccia with bleached angular clasts in a matrix of minute black tourmaline needles. Tourmalinite has been reported from several localities in the western Cascade Range, where it occurs within and adjacent to Miocene granitic intrusions, and is commonly associated with porphyry-copper deposits or base- and precious-metal-bearing hydrothermal-breccia-pipes (Buddington and Callaghan, 1936; Moen, 1977; Hollister, 1979; Evarts and Ashley, 1993; Cummings and others, 1990).

## NEOGENE FILL OF THE PORTLAND BASIN: THE TROUTDALE FORMATION AND SANDY RIVER MUDSTONE

The dissected, southwest-sloping surface in the southwest part of the Ariel quadrangle, part of what Mundorff (1964) called the Troutdale bench, is underlain by deeply weathered basalt-clast conglomerate (Ttf) that stratigraphically overlies a sequence of fine-grained sedimentary rocks (Tsr). Well logs indicate that these sedimentary deposits extend eastward beneath the Pleistocene drift. Mundorff (1964) and Howard (2002) assigned both rock types to the Troutdale Formation of Hodge (1938). In the adjacent Woodland quadrangle, Evarts (2004) mapped the conglomeratic deposits as Troutdale Formation but assigned the subjacent fine-grained strata to the Sandy River Mudstone of Trimble (1963) and this usage is followed here (fig. 3).

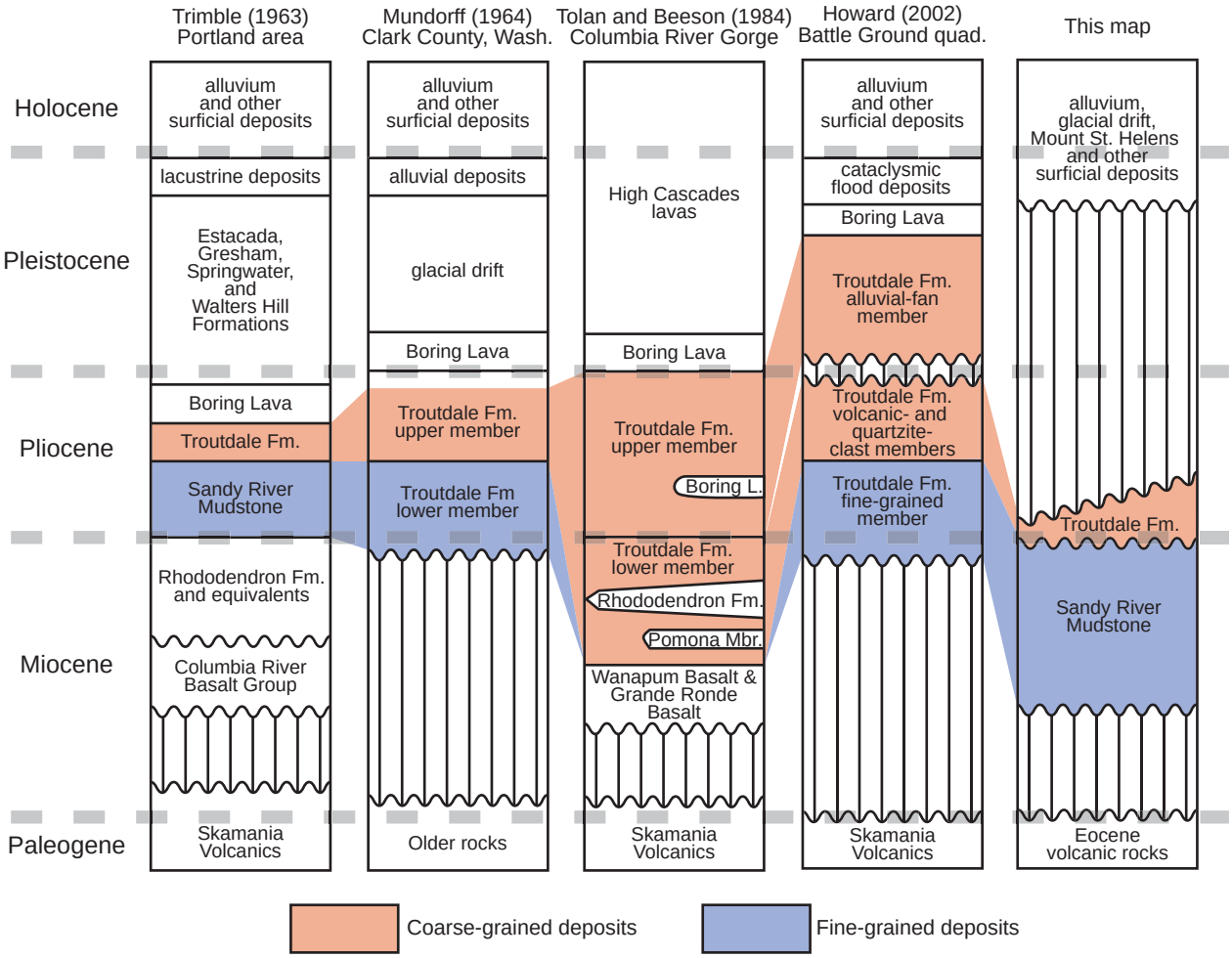


**Figure 3.** Comparison of stratigraphic nomenclature and age assignments for Neogene basin-fill units of the Portland Basin and vicinity.

The Troutdale Formation and Sandy River Mudstone constitute most of the Neogene fill of the Portland Basin (Swanson and others, 1993). Surface exposures and numerous water-well logs indicate that these Neogene sedimentary rocks were deposited on an eroded bedrock surface of considerable relief. The bedrock-surface map of Swanson and others (1993) indicates that the Paleogene bedrock surface slopes south from Bald Mountain and is near sea level at the southwest corner of the Ariel quadrangle, where Troutdale Formation conglomerate composes the upper one-third of the approximately 180-m-thick section of sedimentary strata. The conglomerate is intensely weathered to depths exceeding 30 m, and most exposures consist of red-brown clayey soil with no vestige of the

original texture and stratification. Better exposures to the south and west show that the Troutdale Formation consists of weakly cemented pebble and cobble conglomerate and rare thin lenses of basaltic sandstone and grit (Mundorff, 1964; Evarts, 2004; Howard, 2002). Nearly all clasts are well rounded. Most are virtually aphyric basalts of the Columbia River Basalt Group; the remainder includes light-colored granitic and quartzofeldspathic metamorphic rocks, Fe-oxide stained quartzite, and variable proportions of volcanic rocks eroded from the Cascade Range. The plutonic and metamorphic rocks are foreign to western Oregon and Washington and must have been transported by the ancestral Columbia River from pre-Tertiary terranes east of the Cascade Range. Sedimentological characteristics of the conglomerate, such as the massive to crudely stratified beds, clast-support, openwork and sand-matrix textures, moderate to good sorting, and clast imbrication, are consistent with deposition during flood stage in a gravelly braided river system (Miall, 1977, 1996; Rust, 1978).

In the adjacent Battle Ground quadrangle to the south, Howard (2002) mapped informal quartzite-clast and volcanic-clast members of the Troutdale Formation that corresponds to the Columbian facies and Cascadian facies of the Troutdale Formation, respectively, as defined by Tolan and Beeson (1984). This distinction was not possible in the Ariel quadrangle because, in the rare exposures available, the conglomerate consists almost entirely of aphyric basalt clasts and contains few locally derived volcanic rocks and little or no quartzite.

The Sandy River Mudstone is poorly exposed in the Lockwood and Riley Creek drainages near the southwestern corner of the map area and its distribution is known only from drill holes. Outcrops in the Battle Ground, Woodland, and Ridgefield quadrangles show that the formation consists of well-bedded sandstone, siltstone, and mudstone that typically display graded bedding, planar and trough cross-beds, and cut and fill structures indicative of a fluvial depositional setting (Mundorff, 1964; Evarts, 2004; Howard, 2002; R.C. Evarts, unpub. mapping). Most of the sandy beds are micaceous lithic and arkosic sandstones. Claystone beds, commonly carbonaceous and tuffaceous in part, increase in abundance downsection. A few interbeds of pebbly conglomerate are present in the upper part of the unit, but the contact with the superjacent Troutdale Formation is remarkably abrupt and probably disconformable.

The age of the Troutdale Formation and Sandy River Mudstone in the map area is poorly known, as no dateable beds have been found in this or adjacent quadrangles. Fossil floras collected from the type areas of the two formations near Troutdale, Oregon, suggest that the conformable contact there approximates the Miocene-Pliocene boundary (Trimble, 1963; Mundorff, 1964, Tolan and Beeson, 1984). However, owing to major facies changes (Swanson and others, 1993; Bet and Rosner, 1993), the two units as mapped in the Ariel quadrangle may not be entirely coeval with the exposures near Troutdale. Furthermore, the contact in the northern Portland Basin is commonly an erosional unconformity that records a depositional hiatus of unknown duration, and relations in the Woodland quadrangle to the west of the map area (Evarts, 2004) demonstrate that the Sandy River Mudstone there is in part older than the approximately 15-million-year-old Grande Ronde Basalt. Therefore, Sandy River Mudstone in the map area is assigned a Miocene age. Conglomerate of the overlying Troutdale Formation in the Ariel quadrangle does not contain clasts of olivine-phyric high-alumina basalt and thus is lithologically similar to the lower member of the Troutdale Formation of Tolan and Beeson (1984) in the Columbia River Gorge, which is probably late Miocene and (or) early Pliocene (fig. 3).

## QUATERNARY DEPOSITS

The Lewis River Basin occupies about 3000 $km^2$ of the southern Washington Cascade Range. The river heads on the stratovolcano of Mount Adams, about 85 km east-northeast of the map area, and drains the southern flank of Mount St. Helens. As noted by Major and Scott (1988), Quaternary sedimentation in the lower Lewis River valley has been influenced by several processes, chief of which are: (1) variations in base level owing to sea level fluctuation; (2) episodes of mountain glaciation; (3) inundation by cataclysmic jökulhlaups (glacier-outburst floods); and (4) eruptive activity at the stratovolcanoes.

### GLACIAL AND RELATED DEPOSITS

Several times during the Pleistocene epoch, icecaps covered the Washington Cascade Range and glaciers moved down all of the major river valleys. From examinations of glacial deposits near Mount Rainier, Crandell and Miller (1974) inferred four major glacial episodes, each of which apparently consisted of several lesser advances and retreats (Dethier, 1988). The most widespread glacial deposits in the Cascade Range constitute the Hayden

Creek Drift of Crandell and Miller (1974). Deeply weathered older deposits, the Wingate Hill Drift and the Logan Hill Formation, are locally preserved in the western Cascade foothills in areas beyond the reach of Hayden Creek glaciers. The last major glaciation in western Washington was the late Wisconsinan Fraser glaciation. Deposits of this age in the Cascade Range, named the Evans Creek Drift, are much less extensive than those of the Hayden Creek age (Crandell and Miller, 1974; Crandell, 1987). Widely distributed till and glaciofluvial sediments in the lower Lewis River valley were named the Amboy Drift by Mundorff (1984), who correlated them with the Hayden Creek Drift of the Mount Rainier region on the basis of similar weathering characteristics. Crandell (1987) noted that some of the till in Mundorff's (1984) Amboy Drift, however, was more deeply weathered than typical Hayden Creek Drift and suggested that the Amboy Drift as mapped by Mundorff (1964, 1984) includes some older drift (Crandell, 1987; see also Howard, 2002). In the Ariel quadrangle, unconsolidated deposits that were assigned to the Amboy Drift by Mundorff (1984) also exhibit significant variations in their degree of weathering as well as small but important differences in clast compositions. The Amboy Drift of Mundorff (1984) appears to represent at least two periods of glaciation, one of which predates the Hayden Creek advance. The Amboy Drift as shown on this map is restricted to deposits considered correlative with the Hayden Creek Drift of Crandell and Miller (1974). The older, more deeply weathered drift is herein informally named the drift of Mason Creek.

The drift of Mason Creek consists of moderately to intensely weathered till, stratified drift, and outwash as much as 30 m thick deposited beyond the limits of the younger Amboy Drift. Till and local stratified drift (Qmt) form a continuous blanket on Troutdale Formation gravel south of Bald Mountain and scattered patches in the Lewis River valley at elevations higher than the highest outcrops of Amboy till. The till blanket in the southern part of the map area continues southward as far as the East Fork Lewis River in the Battle Ground quadrangle (Howard, 2002), where it is best exposed in roadcuts in the valley of Mason Creek, one of which, about 1.4 km south of the Ariel quadrangle, was described by Crandell (1987; note that the roadcut location given by Crandell is incorrect; see Howard, 2002). An arcuate ridge that extends south from Bald Mountain and approximates the western limit of the till may be an end moraine. Probable outwash deposits (Qmo) with weathering characteristics similar to those of the pre-Amboy drift south of Bald Mountain form scattered terrace remnants along Cedar Creek and the Lewis River downstream from the western limit of Amboy-age till. Comparable terraces, mapped as older outwash deposits by Evarts (2004), flank the Lewis River almost to its confluence with the Columbia River. Terrace-surface elevations range between about 400 and 700 ft (120 and 215 m). In addition to its topographic position and more intensely weathered condition, the drift of Mason Creek is distinguished from the Amboy Drift by the absence of biotite-bearing dacitic clasts derived from the ancestral Mount St. Helens volcanic center. Most clasts in the drift of Mason Creek consist of Tertiary volcanic rocks eroded from the Cascade Range, but pebbles and cobbles of Columbia River Basalt Group lavas and of quartzite, incorporated from the underlying Troutdale Formation, are locally common. Cobbles of olivine-phyric basalt or basaltic andesite, which were probably eroded from middle Pleistocene monogenetic volcanic centers in the Lewis River drainage upstream from the map area (Evarts and Ashley, 1990a, 1991), are a minor but persistent component in the till (Qmt). Whole-rock $^{40}Ar/^{39}Ar$ ages of these mafic centers range from 622 to 779 ka (R.J. Fleck, written commun., 2003, 2004), which provides a maximum age for the drift of Mason Creek. Weathering characteristics, particularly the thickness of weathering rinds on volcanic clasts, generally resemble those of the Wingate Hill Drift of Crandell and Miller (1974), estimated to be from 300 to 600 ka (Colman and Pierce, 1981; Dethier, 1988). Crandell (1987) suggested that the till along Mason Creek may be slightly older than the type Wingate Hill Drift, hence the drift of Mason Creek may represent more than one Early to Middle Pleistocene glacial advance.

At least 7 m of cobbly pebble gravel, sand, and clayey silt (Qgj) cap the interfluves between Johnson Creek and Colvin Creek between about 800 and 1000 ft (260 and 305 m) elevation. Clasts in the crudely bedded deposit range from subrounded to angular and consist of entirely of indigenous bedrock types. The dominant coarse-grained beds are clast supported but poorly sorted and texturally resemble hyperconcentrated flood-flow deposits (Smith, 1986). The texturally immature alluvium most likely was transported by local creeks rather than in the Lewis River. The anomalous perched position of these deposits, about 125 m above modern creekbeds, suggests deposition probably occurred when the lower reaches of Johnson and Colvin Creeks were blocked by a glacier in the Lewis River valley. The alluvium is located at least 65 m higher than the nearest outcrops of the Amboy Drift, and is more deeply weathered. It is tentatively correlated with the older and somewhat greater glacial advance recorded by the drift of Mason Creek.

The Amboy Drift in the Ariel quadrangle includes till, stratified drift, outwash, and ice-contact deposits with weathering characteristics similar to the Hayden Creek Drift of Crandell and Miller (1974; Mundorff, 1984; Crandell, 1987). Contiguous glacial deposits to the east were correlated with the Hayden Creek Drift by Mundorff

(1984), Crandell (1987), and Evarts and Ashley (1990a, 1991). An extensive mantle of Amboy till (Qat) covers much of the eastern third of the map area to elevations as high as 1750 ft (530 m). A conspicuous pair of moraines west of Fargher Lake marks the limit of the Amboy advance in that area. No end moraine has been recognized in the Lewis River valley but the distribution of Amboy-age till indicates the glacial lobe terminated near Colvin Creek. The low-elevation terrain between Pup Creek and Fargher Lake exhibits a distinctive topography of elongate bedrock hills (rock drumlins) that rise above the till cover. The hills consist of south-dipping lava flows and were sculpted as ice moved westward, parallel to strike, and preferentially quarried out the less resistant interbedded volcaniclastic strata. Many Amboy till outcrops contain minor but conspicuous clasts of light-colored, coarsely porphyritic dacite that bear phenocrysts of quartz, cummingtonite, and biotite; such clasts are particularly common in outcrops north of the Lewis River. Other outcrops lack dacite clasts but contain the same three minerals in the silty and sandy till matrix. The only known source in the Lewis River drainage for this distinctive rock type is the ancestral volcanic center at Mount St. Helens.

Deposits of stratified gravel and sand form a complex assemblage of terraces in both the Lewis River and Cedar Creek valleys. These beds (Qao) locally overlie Amboy till and in places are inset against older and more weathered surficial deposits. Clast types and weathering characteristics are similar to those of the Amboy till, and the sediments are interpreted as glaciofluvial outwash deposited during retreat of Lewis River glacier in late Pleistocene time. Elevations of terrace treads underlain by outwash in the Lewis River valley range from about 700 ft (215 m) near the northeast corner of the quadrangle to 300 ft (90 m) or less near the mouth of Cedar Creek. A nearly continuous outwash-terrace surface along the south side of Cedar Creek valley declines in elevation from 450 ft (135 m) in the east to about 300 ft (90 m) near the creek mouth where it merges with the Lewis River terrace surface. In several places, most conspicuously at Etna, multiple terrace surfaces are evident in Amboy outwash as mapped. The lower terraces are much less dissected than the higher ones. It is unclear whether younger terrace surfaces are erosional features cut into the older outwash deposits or instead record younger episodes of aggradation during an extended, multi-phase, Amboy (Hayden Creek) glaciation such as inferred from deposits in the lower Cowlitz River valley by Dethier (1988). Amboy-age outwash-terrace surfaces below 300 ft (90 m) elevation are veneered with cataclysmic flood deposits (Qfs).

Lake beds (Ql) related to the Amboy Drift are present in several places in the Ariel quadrangle. Deposits beneath the drained lakebed at Fargher Lake accumulated in a proglacial lake impounded by Amboy-age terminal moraines; the lake gradually filled with more than 11 m of organic-rich sand, mud, and peat, punctuated by tephra layers that record eruptions at Mount St. Helens (Rigg, 1958; Heusser and Heusser, 1980; Doh and Steele, 1983; Grigg and Whitlock, 2002). Lake beds are exposed in the south bank of Cedar Creek north-northeast of Bald Mountain. They consist of about 10 to 12 m of dark gray, rhythmically laminated silt and clay. The beds vary in attitude from subhorizontal to subvertical over a distance of 20 m and are unconformably overlain by limonite-cemented cobbly gravel that contains rip-up clasts of varved clay. The small lake in which the rhythmites accumulated probably formed when ice from the Lewis River glacier spilled over into and blocked Cedar Creek; this must have occurred when the glacier was at or near its maximum extent. Scattered angular blocks of andesite as large as 3 m across that now rest on nearby modern alluvium may be ice-rafted erratics. Another small area of lake deposits is inferred to exist about 3.5 km north of Fargher Lake, where a landslide apparently blocked a tributary of Cedar Creek. These deposits are not exposed.

The numerical ages of Hayden Creek Drift and its local equivalent, the Amboy Drift, are poorly known. Estimates range from 60 ka to greater than 300 ka (Crandell and Miller, 1974; Colman and Pierce, 1981; Crandell, 1987; Dethier, 1988). Several observations in the Ariel quadrangle contribute useful constraints on the age of the Amboy Drift. The terminal moraines about 3 km west of Fargher Lake indicate that the area was last occupied by ice near the maximum advance of the Amboy-age glacier. The lower part of an 11-m-deep piston core taken from the drained lakebed contains an interval of laminated inorganic clay interpreted by Grigg and Whitlock (2002) to have formed in an ice-marginal or meltwater-fed lake. They estimated the age of the periglacial beds to be about 55 ka, corresponding to marine oxygen-isotope stage (MIS) 3, which extended from approximately 60 to 27.6 ka (Martinson and others, 1987). This implies that the Amboy till in the Fargher Lake area was deposited during the preceding glacial period corresponding to MIS 4 (74 to 60 ka; Martinson and others, 1987). However, the piston core neither penetrated till nor intersected bedrock. Consequently, the core data provide only a minimum age for the glacial maximum recorded by the nearby Amboy-age moraines.

At many localities in the Lewis River valley, the Amboy Drift (correlative with the Hayden Creek Drift of Crandell and Miller, 1974) is overlain by quartz + biotite ± cummingtonite-bearing tephra (Mundorff, 1984; R.C. Evarts, unpub. mapping) that is mineralogically similar to tephra set C of Mullineaux (1996). This tephra set erupted

from an ancestral Mount St. Helens volcanic center during the Ape Canyon eruptive stage, which extended from about 36,000 to 50,000 $^{14}C$ years B.P. (fig. 4). Crandell (1987) described an exposure near Mount St. Helens where tephra set C rests on weathered till that he assigned to the Hayden Creek Drift. He suggested that an interval of perhaps 15,000 years separated deposition of the till and initiation of the Ape Canyon eruptive stage, and correlated the Hayden Creek glaciation with MIS 4.

Evidence that the Amboy Drift may be much older than MIS 4 comes from the $^{40}Ar/^{39}Ar$ age of 269±13 ka for inferred syneruptive ice-contact deposits (discussed below) in the valley of Cape Horn Creek that were deposited when the Amboy-age Lewis River glacier was near its maximum extent. This age corresponds to MIS 8, about 245 to 300? ka (Martinson and others, 1987). It is considered to be the best age estimate for the Amboy Drift because the other data cited yield only minimum ages and were partly based on assumptions regarding the history of the Mount St. Helens volcanic center that are now known to be incorrect. Alternatively, the deposits mapped as Amboy Drift may be diachronous and were actually deposited during two or more glacial pulses of the Hayden Creek glaciation. This would be consistent with the multiple Hayden Creek advances inferred by Dethier (1988) from an analyses of outwash-terrace deposits in the Cowlitz River valley about 65 km north of the Ariel quadrangle.

## BASALTIC HYALOCLASTITE

Small deposits of basaltic hyaloclastite (Qbh) overlie Amboy Drift along the north shore of Lake Merwin near the mouth of Cape Horn Creek. A similar deposit forms a small terrace on the opposite shore of the lake. The deposits consist mostly of angular clasts of black vitric basalt that rarely exceed 1 cm in diameter. Rounded pebbles and cobbles of Tertiary bedrock are dispersed through the hyaloclastite and locally concentrated in gravel lenses with a matrix of coarse basaltic sand; the proportion of rounded Tertiary clasts is higher in the outcrop on the south lakeshore. As viewed in thin section, the basalt clasts consist of pale brown, moderately vesicular to nonvesicular sideromelane that contains olivine and plagioclase phenocrysts and is partially replaced by yellow palagonite. The hyaloclastite near Cape Horn Creek forms a north-thickening wedge as thick as 10 m. Crude stratification dips variably southward at 20° to 70°. Contact relations with the subjacent drift vary; in one outcrop the hyaloclastite rests conformably on south-dipping stratified drift, whereas nearby it pinches out against an erosional unconformity developed in till and laminated silt. At one locality, the hyaloclastite contains angular rip-up clasts of silt as large as 50 cm across. The hyaloclastite is unconformably overlain by outwash gravel (Qao) or by alluvial and lahar deposits dominated by Mount St. Helens dacitic debris of Ape Canyon age (Qsa).

The deposit appears to constitute the remains of an apron of phreatomagmatically generated debris that may have filled the lower part of Cape Horn Creek and extended across the Lewis River valley floor. The presence of scattered rounded clasts and gravel interbeds dominated by older rocks indicates deposition in a stream, although the angular character of the basalt clasts signifies limited transport. South-dipping stratification in the hyaloclastite on the north shore of Lake Merwin suggests deposition on a southward prograding delta front where Cape Horn Creek entered a lake. Alternatively, the hyaloclastite may reflect explosive interaction of lava with melted glacial ice and deposition in a subglacial channel. The source vent for the hyaloclastite, presumably nearby, has not been located. No other exposures of basaltic sand have been observed in the area, and the chemistry of the basalt clasts (table 1, no. 58; A.M. Sarna-Wojcicki, written commun., 2000) does not resemble that of any of the known Quaternary basalts in this part of the Lewis River valley (Evarts and Ashley, 1990a, 1991).

## DEPOSITS DERIVED FROM THE MOUNT ST. HELENS VOLCANIC CENTER

The Lewis River drains the southern slope of Mount St. Helens. Explosive eruptions at the volcanic center delivered large quantities of dacitic debris in the form of pyroclastic flows and lahars to the river during the late Pleistocene and Holocene (Crandell, 1987; Major and Scott, 1988); in postglacial time, eruptive activity at the volcano has been the dominant influence on sedimentation in the Lewis River valley. The periodic influx of volcaniclastic debris triggered major aggradational episodes downstream, and the deposits of these approximately syneruptive events constitute a major part of the late Quaternary record in the lower Lewis River valley. Crandell (1987) has shown that Mount St. Helens eruptive activity was episodic and can be divided into several eruptive stages and periods (fig. 4). Based chiefly on stratigraphic position and lithologic characteristics, Mount St. Helens-derived deposits in the Ariel quadrangle are divided into three groups corresponding in part to Crandell's eruptive history for Mount St. Helens: (1) deposits of the Swift Creek eruptive stage (Qssw), (2) deposits of the Ape Canyon eruptive stage (Qsa), and (3) deposits significantly older than the Ape Canyon eruptive stage of Crandell (Qso).

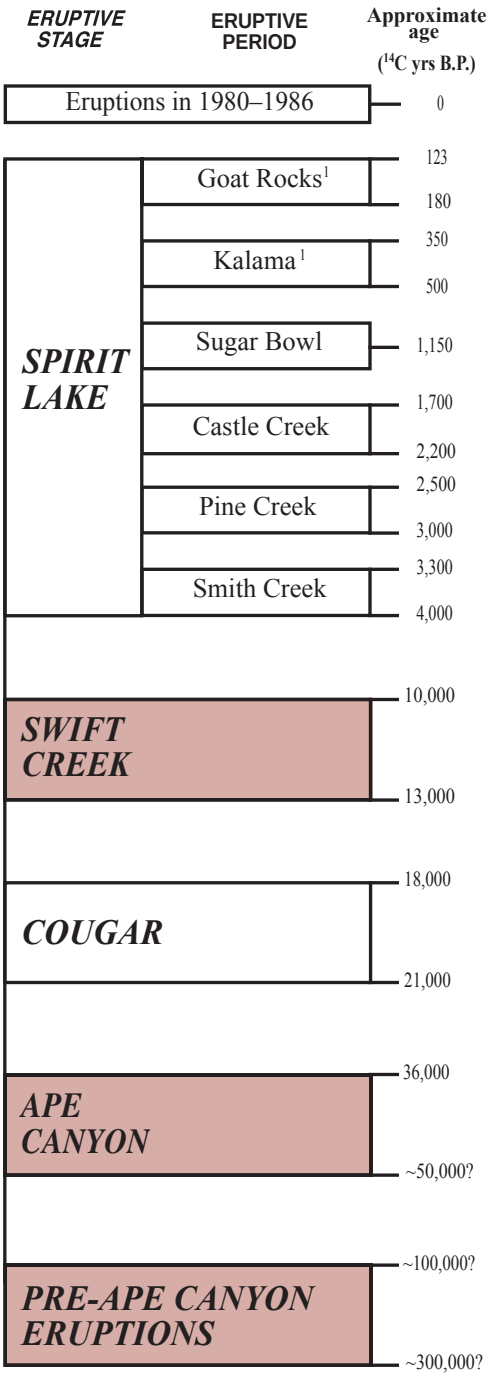


**Figure 4.** Eruptive stages and eruptive periods of Mount St. Helens volcano, modified from Crandell (1987). Shaded boxes designate stages corresponding to mapped deposits in the Ariel 7.5' quadrangle.

Small remnants of alluvial and possible debris-flow deposits (Qso) composed mostly of light-colored, coarsely porphyritic dacite have been found adhering to the valley walls well above modern streambeds at scattered

locations in the Ariel quadrangle and areas to the east (Evarts and others, 2003). Outcrops in this quadrangle are found at 800 ft (245 m) in Husky Creek, 1000 ft (300 m) along Pup Creek, and 1500 ft (460 m) in the valley of Cape Horn Creek. The volcaniclastic deposits overlie Amboy Drift at all three locations. The largest deposit is that in Cape Horn Creek and comprises as much as 9 m of well bedded silt, sand, and gravel. Most beds are a few centimeters thick, but thin varve-like clay and silt beds and thicker probable debris-flow deposits, with prismatically-jointed dacite clasts as large as 25 cm across, are also present. Material coarser than silt size consists almost exclusively of lithic and pumiceous dacite and crystals in widely varying proportions. Dacite clasts contain abundant large phenocrysts of quartz, plagioclase, biotite, and cummingtonite; well-sorted crystal-rich sandy interbeds are mineralogically similar. The crystals are generally fresh but all of the original dacitic glass has been thoroughly weathered to pale yellow to orange-brown clay. The only plausible source for the dacitic debris in these deposits is the volcanic center of Mount St. Helens; the dacite clasts closely resemble rocks erupted from the volcano during its earliest recognized period of activity, the Ape Canyon eruptive stage of Crandell (1987), and are readily distinguished from Paleogene silicic rocks. The paucity of Tertiary rock fragments indicates these are not typical fluvial sediments of the Lewis River system, and the elevations of the deposits are much too high for them to be erosional remnant of a valley-wide fill. Instead, the sediments consist of freshly erupted dacitic material that was transported downstream when the valley was filled with ice, and accumulated, probably in small lakes, between the glacier margin and adjacent valley walls. Evidently, a major eruptive episode at ancestral Mount St. Helens during Amboy time temporarily overwhelmed the Lewis River drainage with dacitic debris and generated a great pulse of sedimentation in the ice-filled Lewis valley. A flood of hot juvenile dacitic debris probably mixed with melting ice and snow on the volcano's slopes to generate lahars that moved along and across the surface of the glacier and deposited loose debris that was rapidly reworked. Transport across the glacier surface minimized mixing with detritus eroded from Tertiary bedrock. Some of these sediments were trapped and preserved in a small lake in the valley of Cape Horn Creek. The observed 15° downslope dip of the beds, as well as minor soft-sediment deformation and local unconformities, probably reflect removal of support as ice melted during retreat of the Lewis River glacier. The ice-contact deposits are located only about 30 m lower than the highest nearby occurrence of till, so are inferred to have accumulated near the Amboy glacial maximum.

The Ape Canyon eruptive stage of Mount St. Helens as defined by Crandell (1987) postdates the Hayden Creek Drift. Although the clasts in the ice-contact deposits of the Ariel quadrangle are lithologically similar to dacites produced during the Ape Canyon eruptive stage, the synglacial deposits described here (Qso) apparently record older eruptive activity, the evidence for which has been removed from the area near the volcano. Other evidence in the lower Lewis River valley for eruptive activity at Mount St. Helens before or during the Hayden Creek (Amboy) glaciation includes (1) the presence of Ape-Canyon-type dacite clasts in Amboy till; (2) interbeds of relatively uncontaminated Mount St. Helens-derived sands in Amboy outwash gravels; and (3) tephra deposits lying beneath till at two locations in the adjacent Amboy quadrangle (R.C. Evarts, unpub. mapping). Furthermore, an $^{40}Ar/^{39}Ar$ age of approximately 269±13 ka (table 2) was obtained on plagioclase extracted from pumice lapilli at the Cape Horn Creek locality, much older than the 36,000 to 50,000 $^{14}C$ years B.P. inferred for the Ape Canyon eruptive stage by Crandell (1987). Recent stratigraphic and geochronologic investigations at Mount St. Helens (M.A. Clynne, written commun., 2002; Evarts and others, 2003) and in eastern Washington (Berger and Busacca, 1995; Whitlock and others, 2000) indicate that the volcanic center has a history extending back as far as 300 ka.

Deposits of probable Ape Canyon age (Qsa), correlative with the post-Hayden Creek deposits near Mount St. Helens, are exposed at several places along the north shore of Lake Merwin east of Cape Horn Creek; similar deposits crop out in the steep valley walls of lower Johnson Creek about 1.5 km above its mouth. In both areas the deposits overlie Amboy Drift (Qat and Qao) or Tertiary bedrock. The unit consists of pebbly to bouldery diamicts of probable lahar origin interbedded with fluvially deposited sand and gravel. Clasts in the diamicts are chiefly distinctive coarsely porphyritic quartz- and biotite-bearing dacite of the kind erupted from Mount St. Helens during the Ape Canyon eruptive stage; no clasts definitely attributable to younger eruptive episodes are present (M.A. Clynne, oral commun., 2003). The alluvial beds are compositionally similar but contain minor proportions of Tertiary rocks, and are presumably reworked from penecontemporaneous lahar deposits.

Deposits probably emplaced during the Swift Creek eruptive stage (Qssw) of Mount St. Helens (10,000 to 13,000 $^{14}C$ years B.P.; fig. 4) are exposed north of the Lewis River downvalley from Merwin Dam. An exceptionally coarse-grained diamict crops out at the base of the sequence directly west of Merwin Dam. The matrix-poor, bouldery diamict contains abundant rounded clasts, some as large as 2 m across, of hornblende-hypersthene dacite (table 1, no. 59) that was probably erupted during the Swift Creek eruptive stage (M.A. Clynne, written commun., 2003). The diamict was most likely deposited by a lahar initiated when heavy rainfall on the

volcano's flank remobilized proximal alluvium. Pebbly lahar and lahar-runout deposits mantle the slope above the diamict (Major and Scott, 1988). They contain lithic clasts compositionally similar to those in the underlying diamict as well as pumice that mineralogically resembles tephra set S of early Swift Creek age (Mullineaux, 1996). Similar deposits that crop out near the mouth of Colvin Creek are overlain by Missoula-flood silts (Qfs). The compositional and stratigraphic evidence indicates that these deposits are of Swift Creek age.

A buried paleochannel beneath the gently sloping surface northwest of Merwin Dam (I.A. Williams, unpub. report, 1930; Tilford and Sullivan, 1981), is filled with poorly sorted deposits of probable glacial or lahar origin. Most of this fill is likely similar in age to the deposits below the dam, although a thin, fine-grained, slope-mantling lahar at the top of the sequence may have been deposited during the younger Spirit Lake eruptive stage (Major and Scott, 1988).

## CATACLYSMIC FLOOD DEPOSITS

During the last glacial maximum in late Pleistocene time, an ice dam at Pleistocene Lake Missoula in western Montana failed repeatedly, and each collapse generated enormous floods or jökulhlaups, commonly referred to as the Missoula floods, that coursed down the Columbia River and into the Portland Basin (Bretz, 1925, 1959; Bretz and others, 1956; Trimble, 1963; Allison, 1978; Baker and Bunker, 1985; Waitt, 1985, 1994, 1996; O'Connor and Baker, 1992; Benito and O'Connor, 2003). The sediment-laden floodwaters were hydraulically constricted by the narrow reach of the Columbia River valley north of Woodland. The constriction caused temporary ponding in the Portland Basin and tributary valleys to levels as high as 400 ft (120 m). Radiocarbon ages, paleomagnetic measurements, and tephrochronologic data indicate that the last glacial episode of floods occurred chiefly between about 17,000 and 13,000 $^{14}$C years B.P. (Waitt, 1985, 1994; Atwater, 1986; Clague and others, 2003). Similar episodes of cataclysmic flooding probably occurred earlier in the Quaternary (McDonald and Busacca, 1988; Zuffa and others, 2000; Bjornstad and others, 2001).

During each flood, the suspended load of fine sand and silt settled out of the temporarily ponded floodwaters. In the northern Portland Basin, multiple floods (Waitt, 1994, 1996) collectively built up deposits of laminated micaceous sediments as thick as 30 m. In the Ariel quadrangle, silty slack-water flood deposits (Qfs) as thick as 5 m blanket terrace surfaces at elevations as high as 300 ft (90 m ) along the Lewis River and lower Cedar Creek. The laminated character of the flood deposits is obvious only in fresh slump-scarp outcrops because oxidation colors exposures light brown and obscures bedding. They are dominated by grains of quartz and feldspars and contain conspicuous muscovite, which confirms their Columbia River provenance.

## HOLOCENE ALLUVIAL DEPOSITS

Unconsolidated alluvium (Qa) forms local and ephemeral accumulations along many of the bedrock-confined tributaries of the Lewis River and Cedar Creek. More extensive but thinner deposits overlie outwash along Cedar Creek. The Lewis River flows between cliffs of Paleogene bedrock less than 100 m apart for much of its reach downstream from Merwin Dam, and active alluvium is confined to local bars along the river's edge. Excavation for the dam revealed the existence of a sediment-filled slot incised into bedrock below modern river level; this channel is about 20 m wide and its floor lies at 20 m below sea level (I.A. Williams, unpub. report, 1930; Tilford and Sullivan, 1981). Water-well logs from sites a few kilometers west of the Ariel quadrangle show that at least 75 m of unconsolidated sediment underlies the valley floor there. The buried Lewis River paleochannel was probably carved when local base level was lowered in response to the drop in sea level during the last glacial maximum (Warne and Stanley, 1995; Clark and Mix, 2002), and filled with sediment as sea level rose in latest Pleistocene and Holocene time. This fill consists largely of sand and gravel, including some pumice-bearing beds and boulders (I.A. Williams, unpub. report, 1930). Dacitic debris delivered to the Lewis River by eruptions at Mount St. Helens may constitute a substantial proportion of this sediment.

Upstream from the bedrock constriction at Merwin Dam, the Lewis River valley floor abruptly widens. Prior to inundation by the reservoir, the river meandered across a floodplain between 0.5 and 1.4 km wide that slopes gently downvalley from an elevation of about 100 ft (30 m) at the eastern boundary of the Ariel quadrangle to 70 ft (20 m) near the dam site. The age and composition of deposits beneath this flooded surface are unknown, but exposures upstream and downstream of Lake Merwin indicate that they postdate the Smith Creek eruptive period of Mount St. Helens (see fig. 4). Large quantities of volcaniclastic debris were dumped into the Lewis River

during the Pine Creek eruptive period (about 3000-2500 radiocarbon years B.P.; Crandell, 1987) and at least the upper part of the submerged fill probably consists of lahar and derivative alluvial deposits of this age.

### LANDSLIDE AND TALUS DEPOSITS

Landslides (Qls) are distributed throughout the steeper terrain of the Ariel quadrangle but are most common in areas that were not glaciated during late Pleistocene time. Many result from failure of weathered, clayey, Paleogene volcaniclastic rocks (Tvs, Tt, and sedimentary interbeds within flow-dominated units Tba and Ta). Others reflect failure of clay-rich hydrothermally altered rock; the large active landslide in Colvin Creek, for example, developed in altered rock adjacent to the ring fault that forms the southern margin of the Davis Peak caldera. Younger poorly lithified deposits are also susceptible to sliding, especially on steeper slopes. The large landslide 3 km northwest of Fargher Lake appears to have resulted from failure of water-saturated till, and temporarily blocked Cedar Creek. Piecemeal breakup of cliff-forming units locally forms talus deposits, most notably on the steep glaciated north flank of Green Mountain. Only the larger landslides are shown on this map; most areas underlain by Quaternary units and the Troutdale Formation contain small slumps and debris-flow deposits that are too small to portray at 1:24,000 scale.

## STRUCTURAL FEATURES

The Ariel quadrangle lies along the northeastern margin of the Portland Basin, part of Puget-Willamette Lowland that separates the Cascade Range to the east from the Oregon and Washington Coast Range to the west. In the Cascade Range of southwestern Washington, structural attitudes of Paleogene strata delineate a set of large-wavelength, south- to southeast-plunging folds that are believed to have developed in late early Miocene time (Evarts and Swanson, 1994). The late Eocene to early Oligocene section in the Ariel quadrangle generally strikes approximately east-west and dips south at 15° to 30°; it is located along the poorly defined synclinal axis of one of these folds. Bedding flattens to the southeast, and the syncline cannot be traced south of Fargher Lake. The dominant structural trend is interrupted by the Davis Peak caldera in the northwestern part of the quadrangle. Attitudes within the caldera are variable and commonly steep and reflect localized deformation associated with caldera-forming processes.

Because of limited outcrop in the map area, compelling evidence for the existence of faults is sparse. Some faults shown on this map are projected from structures observed in roadcuts or natural exposures; others are inferred from apparent discontinuities in distinctive stratigraphic units, from topographic lineaments, or from abrupt changes in bedding trends. Most faults appear to be high-angle normal and strike-slip structures similar to those mapped elsewhere in southwestern Washington (Wells, 1981; Wells and Coe, 1985; Evarts and Ashley, 1991, 1992; Evarts and Swanson, 1994; Evarts, 2002, 2004; R.C. Evarts, unpub. mapping). They are thought to accommodate the paleomagnetically recorded rotations of small crustal blocks in response to long-term oblique convergence along the Cascadia Subduction Zone throughout Cenozoic time (Wells and Coe, 1985; Wells, 1989, 1990; Beck and Burr, 1979; Bates and others, 1981; Hagstrum and others, 1999).

Most faults in the northern half of the Ariel quadrangle are oriented east-northeast, parallel to the abundant dikes. Some dikes were emplaced along the faults; other faults show post-intrusion movement. If, as seems likely, the dikes were emplaced prior to regional folding, then they originally occupied essentially vertical fractures. The preferential strike of the dikes probably reflects the late Eocene to early Oligocene regional tectonic stress regime. Paleomagnetic evidence for roughly 30° of clockwise rotation in the southern Washington Cascade Range during the last 30 to 40 m.y. (Beck and Burr, 1979; Bates and others, 1981; Hagstrum and others, 1999) suggests the dikes were originally oriented about N. 45° E., which probably approximates the maximum regional horizontal compressive stress axis at the time of emplacement (Nakamura, 1977). Plate-motion reconstructions indicate that the azimuth of the convergence direction between the Farallon and North American plates was about N. 45° E. at 35 Ma (Verplanck and Duncan, 1987).

The course of Lewis River below Lake Merwin may be controlled by high-angle faults. A reverse fault is exposed in a gully 350 m south of Merwin Dam, directly south of the outlet of the diversion tunnel through which the Lewis River was routed during construction of the dam. The fault strikes N. 80° E., dips 70° S., and juxtaposes a section of seriate basaltic andesite flows (Tba) to the south over the porphyritic dacite of Marble Creek (Tdm) to the north. The fault surface is coated with clayey gouge and exhibits grooves that indicate primarily dip-

slip motion; throw is at least 50 m. Similarly oriented fault zones with small displacements were encountered during construction of Merwin Dam (I.A. Williams, unpub. report, 1930), and one such fault crops out along the northwest bank of the river below the dam. These fault zones, however, are filled with zeolites and calcite, indicating they are of ancient origin, whereas the reverse fault near the diversion tunnel lacks this mineralization and thus appears to be younger. The time of its most recent movement is unknown, but semiconsolidated outwash gravels of Amboy age that are banked against the fault plane are not disrupted, hence the fault has probably not moved since Pleistocene time. Downstream, a zone of fractured and sheared basaltic andesite (Tba) crops out on the south bank of the Lewis River opposite the mouth of Colvin Creek. The disturbed zone roughly parallels the river, and it may mark the margin of a fault zone that controls the linear, northeast-trending reach of the river upstream from this locality.

## GEOLOGIC EVOLUTION

Paleogene bedrock in the Ariel quadrangle consists of thick lava-flow piles, silicic dome complexes, coarse-grained breccias, pumiceous pyroclastic rocks, and scattered intrusions, and is typical of central vent and proximal volcanic environments within continental volcanic arcs (Williams and McBirney, 1979; Vessell and Davies, 1981; Cas and Wright, 1987; Orton, 1996). Local sections of interbedded pyroclastic deposits, stratified volcaniclastic sedimentary rocks, and isolated lava flows in the southern part of the map area are characteristic of deposition in medial to distal settings beyond the flanks of active volcanic edifices (Williams and McBirney, 1979; Vessell and Davies, 1981). Regional relations indicate that this area was near the western margin of the active Cascade volcanic arc during Paleogene time. Age determinations in this and adjacent quadrangles (Evarts, 2002, 2004; R.J. Fleck, written commun., 2000) show that the extrusive rocks of the map area were emplaced mainly between 37 and 34 Ma, early in volcanic arc history (Duncan and Kulm, 1989; Evarts and Swanson, 1994).

The most prominent event recorded by the Paleogene rocks of the Ariel quadrangle was the development of the volcanic center in the Davis Peak area. Eruptions of mafic to intermediate-composition lavas probably built a large composite stratovolcano similar to those that dominate the modern Cascade Range. This early activity was followed by emplacement of one or more large dacitic domes, preserved as the dacite of Marble Creek, at or near the volcano's summit. Volcanism culminated in a paroxysmal eruption of dacitic pyroclastic debris and subsequent edifice collapse at about 35 Ma to form the oldest and westernmost known caldera in the Washington Cascade Range. Intermediate- to silicic-composition postcaldera magmas intruded the caldera, its margins, and the surrounding area. Some of these intrusions may occupy feeder systems for late Eocene or Oligocene volcanoes that have since been eroded away, but the strong preferred orientation of the postcaldera dikes indicates that the regional tectonic stress field rather than local volcanic forces exercised primary control on dike emplacement. The N. 45°E. orientation (after correcting for paleomagnetically inferred clockwise rotation), which probably approximates the maximum horizontal compressive stress (Nakamura, 1977), parallels the azimuth of late Paleogene Farallon-North America plate convergence (Wells and others, 1984; Verplanck and Duncan, 1987). Vigorous volcanic activity continued along the Cascade volcanic arc into early Miocene time. A precipitous decline in volcanism after about 17 Ma in southern Washington corresponds to a region-wide episode of uplift, folding, and erosion (Evarts and Swanson, 1994).

Development of the Portland Basin apparently began at about the same time as the early Miocene regional deformation in the Cascade arc (Beeson and Tolan, 1990; Beeson and others, 1989). The older basin-fill deposits are predominantly fine-grained fluvial and lacustrine beds of the Sandy River Mudstone; as much as 400 m of these middle to late Miocene sediments accumulated as the floor of the Portland Basin gradually subsided (Trimble, 1963; Mundorff, 1964; Swanson and others, 1993). The absence of coarse-grained volcaniclastic debris signifies that the middle Miocene Cascade arc was topographically subdued and volcanically quiescent compared to earlier times. To the southeast near the western end of the Columbia River Gorge, the fine-grained strata grade laterally into conglomeratic deposits (Tolan and Beeson, 1984; Swanson and others, 1993; Bet and Rosner, 1993). In the Ariel quadrangle and throughout the northern Portland Basin, the fine-grained basin-fill strata are overlain by conglomeratic beds assigned to the Troutdale Formation (Trimble, 1963; Mundorff, 1964; Swanson and others, 1993; Evarts, 2002, 2004). The clast compositions of the Sandy River Mudstone and Troutdale Formation indicate that these units mostly consist of material eroded from pre-Tertiary terranes east of the Cascade Range and transported into the basin by an ancestral Columbia River; contributions from volcanic activity in the arc were minor. The marked lithologic change at the contact of the two units records northward progradation of a gravelly braid-plain across the northern Portland Basin during late Miocene or early Pliocene time. This pronounced change

in the Columbia River sedimentary regime may reflect regional uplift to the east and initial incision of the Columbia River Gorge.

The southwestward tilt of the surface of the Troutdale Formation indicates that the Portland Basin continued to develop into Pliocene time. If Troutdale Formation sediments were deposited near sea level, as suggested by Beeson and Tolan (1990), then their present position at elevations near 900 ft (275 m) in the map area implies that uplift of the Cascade Range occurred concurrently with the later stages of basin-floor subsidence. This uplift caused the Columbia River to incise its floodplain and erode the late Miocene to early Pliocene gravel from much of the northern Portland Basin, leaving remnants preserved only on the uplifted basin flanks.

Scattered remnants of Troutdale Formation conglomerate north of the Lewis River in the Woodland quadrangle (Evarts, 2004) show that the Troutdale originally extended northward. Continuing uplift of the Cascade Range rejuvenated an ancestral Lewis River that, by early Pleistocene time, had removed most Troutdale Formation sediments and cut a deep valley into the subjacent bedrock. A complex assemblage of Quaternary deposits in the Lewis River and Cedar Creek valleys records alternating periods of alluviation and downcutting in response to large variations in sediment load and fluctuations in sea level (Mundorff, 1984; Major and Scott, 1988).

Several times during the Pleistocene, mountain glaciers moved out of the Cascade Range and down the Lewis River valley as far as the map area. Much of the evidence for earlier glacial advances was erased by the glaciation that deposited the Amboy Drift, the local equivalent of the Hayden Creek Drift. However, deeply weathered and dissected pre-Amboy glacial deposits, the drift of Mason Creek, underlie a broad area east of Lockwood Creek, and remnants of pre-Amboy outwash terraces and alluvium are scattered in the Lewis River valley in the map area as well as down valley (Evarts, 2004). During Amboy time, a large piedmont glacier issued from the Lewis River valley and spread over the relatively low-lying area along the northeast margin of the Portland Basin (Mundorff, 1984). The ice sheet reached as far west as Colvin Creek in the Lewis River valley and Fargher Lake to the south, leaving behind prominent streamlined ridges (rock drumlins) and thick drift deposits. Evidence in the Ariel quadrangle suggests that the Amboy Drift may include deposits of more than one glacial pulse during the Hayden Creek Stade, with the maximum advance occurring at about 270 ka. The most recent glaciation in the Cascade Range, which culminated about 17,000 $^{14}$C years B.P. (Barnosky, 1984), was considerably less extensive than the Hayden Creek (Amboy) advance and left no identified deposits in the lower Lewis River valley.

The volcanic center at Mount St. Helens first became active at some time before or during the Amboy glaciation and has erupted frequently since (Crandell, 1987). At least one eruption occurred at a time when the Lewis River valley was filled with ice. Many of these eruptions were explosive, and some dumped huge quantities of pyroclastic debris into the Lewis River system. Evidence for periods of eruption-induced aggradation and subsequent incision is abundant in the Ariel quadrangle (Major and Scott, 1988). Most of the deposits of Mount St. Helens origin that are preserved within the quadrangle were deposited by lahars or reworked from primary eruptive deposits upstream. They underlie scattered terrace remnants in the Lewis valley and probably constitute the extensive terraces beneath the surface of Lake Merwin. They are younger than the Amboy Drift, and were largely deposited during the Ape Canyon and Swift Creek eruptive stages of Mount St. Helens, between about 50,000 and 10,000 $^{14}$C years B.P. (Crandell, 1987; fig. 4). Cougar-age deposits are abundant in the Lewis River Valley upstream from the map area (Major and Scott, 1988; M.A. Clynne, oral commun., 2003; R.C. Evarts, unpub. mapping) but none have been identified within the map area.

Terrace surfaces as high as 300 ft (90 m) in the valleys of the Lewis River and Cedar Creek are mantled by as much as several meters of laminated micaceous silt and clay. These are slack-water beds deposited between about 17,000 and 13,000 $^{14}$C yrs B.P. when waters of the cataclysmic Missoula glacier-outburst floods (Bretz, 1959; Waitt, 1985) on the Columbia River temporarily ponded in the Portland Basin and backed up into its tributaries. The bed of the Lewis River was lower at that time, owing to the lower glacial sea level, and as sea level rose, the riverbed aggraded. The resulting postglacial valley fill, now submerged beneath Lake Merwin, likely includes a substantial proportion of volcaniclastic material from Mount St. Helens, particularly that produced during Pine Creek eruptive period of Crandell (1987), 2500-3000 $^{14}$C years B.P. (fig. 4), when the volcano dumped large quantities of dacitic debris into the Lewis River.

## GEOLOGIC RESOURCES

Known geologic resources available in the Ariel quadrangle are limited to nonmetallic industrial materials, chiefly aggregate for construction purposes. Paleogene volcanic bedrock has locally been quarried for crushed

aggregate used primarily as base and surface material for logging roads. Sand and gravel are locally available from unconsolidated alluvial deposits along the Lewis River but are more abundant and accessible downstream from the map area. Peat deposits underlie the drained lakebed north of Fargher Lake (Rigg, 1958). Hydrothermal alteration of the kind observed in the northern half of the quadrangle is commonly associated with metallic mineral deposits in the Cascade Range, but no significant mineral occurrences were found in the map area. The presence of tourmalinite is intriguing, however, because similar alteration is intimately associated with porphyry-copper type mineralization in the St. Helens and Washougal districts in the mountains to the east (Moen, 1977).

## REFERENCES CITED


Allison, I.S., 1978, Late Pleistocene sediments and floods in the Willamette Valley: The Ore Bin, v. 40, p. 177–203.

Atwater, B.F., 1986, Pleistocene glacial-lake deposits of the Sanpoil River Valley, northeastern Washington: U.S. Geological Survey Bulletin 1661, 39 p.

Bacon, C.R., 1983, Eruptive history of Mount Mazama and Crater Lake caldera, Cascade Range, U.S.A.: Journal of Volcanology and Geothermal Research, v. 18, p. 57–115.

Baker, V.R. and Bunker, R.C., 1985, Cataclysmic late Pleistocene flooding from glacial Lake Missoula–a review: Quaternary Science Reviews, v. 4, p. 1–41.

Balsillie, J.H., and Benson, G.T., 1971, Evidence for the Portland Hills Fault: The Ore Bin, v. 33, p. 109–118.

Barnosky, C.W., 1984, Late Pleistocene and early Holocene environmental history of southwestern Washington State, U.S.A.: Canadian Journal of Earth Sciences, v. 21, p. 619–629.

Bates, R.G., Beck, M.E., Jr., and Burmester, R.F., 1981, Tectonic rotations in the Cascade Range of southern Washington: Geology, v. 9, p. 184–189.

Beck, M.E., Jr., and Burr, C.D., 1979, Paleomagnetism and tectonic significance of the Goble Volcanic Series, southwestern Washington: Geology, v. 7, p. 175–179.

Beeson, M.H., Fecht, K.R., Reidel, S.P., and Tolan, T.L., 1985, Regional correlations within the Frenchman Springs Member of the Columbia River Basalt Group—new insights into the middle Miocene tectonics of northwestern Oregon: Oregon Geology, v. 47, p. 87–96.

Beeson, M.H., and Tolan, T.L., 1990, The Columbia River Basalt Group in the Cascade Range: a middle Miocene reference datum for structural analysis: Journal of Geophysical Research, v. 96, p. 19,547–19,559.

Beeson, M.H., Tolan, T.L., and Anderson, J.L., 1989, The Columbia River Basalt Group in western Oregon—geologic structures and other factors that controlled flow emplacement patterns, *in* Reidel, S.P., and Hooper, P.R, eds., Volcanism and tectonism in the Columbia River flood-basalt province: Geologic Society of America Special Paper 239, p. 223–246.

Benito, G., and O'Connor, J.E., 2003, Number and size of last-glacial Missoula floods in the Columbia River valley between the Pasco Basin, Washington and Portland, Oregon: Geological Society of America Bulletin, v. 115, p. 624–638.

Berger, G.W., and Busacca, A.J., 1995, Thermoluminescence dating of late Pleistocene loess and tephra from eastern Washington and southern Oregon and implications for the eruptive history of Mount St. Helens: Journal of Geophysical Research, v. 100, p. 22,361–22,374.

Berggren, W.A., Kent, D.V., Swisher, C., III, Aubry, M.-P., 1995, A revised Cenozoic geochronology and chronostratigraphy, *in* Berggren, W.A., Kent, D.V., Aubry, M.-P., and Hardenbol, J., eds., Geochronology, time scales and global stratigraphic correlation: Society of Economic Paleontologists and Mineralogists Special Publication 54, p. 129–212.

Bet, J.N., and Rosner, M.L., 1993, Geology near Blue Lake County Park, eastern Multnomah County, Oregon: Oregon Geology, v. 55, p. 59–69.

Bjornstad, B.N., Fecht, K.R., and Pluhar, C.J., 2001, Long history of pre-Wisconsin, Ice Age cataclysmic floods—evidence from southeastern Washington State: Journal of Geology, v. 109, p. 695–713.

Blakely, R.J., Wells, R.E., Yelin, T.S., Madin, I.P., and Beeson, M.H., 1995, Tectonic setting of the Portland-Vancouver area, Oregon and Washington—constraints from low-altitude aeromagnetic data: Geological Society of America Bulletin, v. 107, p. 1051–1062.

Bliton, W.S., 1989, Lewis River Projects, *in* Galster, R.W., Coombs, H.A., and Waldron, H.H., eds., Engineering Geology of Washington: Washington Division of Geology and Earth Resources Bulletin 78, v. I, part II, p. 277–296.

Bott, J.D.J., and Wong, I.G., 1993, Historical earthquakes in and around Portland, Oregon: Oregon Geology, v. 55, p. 116–122.
Branney, M.J., 1995, Downsag and extension at calderas–new perspectives on collapse geometries from ice-melt, mining, and volcanic subsidence: Bulletin of Volcanology, v. 57, p. 303–318.
Branney, M.J., and Kokelaar, P., 1994, Volcanotectonic faulting, soft-state deformation, and rheomorphism of tuffs during development of a piecemeal caldera, English Lake District: Geological Society of America Bulletin, v. 106, p. 507–530.
Bretz, J H., 1925, The Spokane flood beyond the Channeled Scablands: Journal of Geology, v. 33, p.97–115, p. 236–259.
Bretz, J H., 1959, Washington's Channeled Scabland: Washington Division of Mines and Geology Bulletin 45, 55. p.
Bretz, J H., Smith, H.T.U., and Neff, G.E., 1956, Channeled Scabland of Washington—new data and interpretations: Geological Society of America Bulletin, v. 67, p. 957–1049.
Buddington, A.F., and Callaghan, E., 1936, Dioritic intrusive rocks and contact metamorphism in the Cascade Range in Oregon: American Journal of Science, Fifth Series, v. 31, p. 421–449.
Cas, R.A.F., and Wright, J.V., 1987, Volcanic successions—modern and ancient: London, Allen and Unwin, 528 p.
Cho, M., Maruyama, S., and Liou, J.G., 1987, An experimental investigation of heulandite-laumontite equilibrium at 1000 to 2000 bar $P_{fluid}$: Contributions to Mineralogy and Petrology, v. 97, p. 43–50.
Clague, J.J., Barendregt, R. Enkin, R.J., and Foit, F.F., Jr., 2003, Paleomagnetic and tephra evidence for tens of Missoula floods in southern Washington: Geology, v. 31, p. 247–250.
Clark, P.U., and Mix, A.C., 2002, Ice sheets and sea level of the Last Glacial Maximum: Quaternary Science Reviews, v. 21, p. 1–7.
Colman, S.M., and Pierce, K.L., 1981, Weathering rinds on andesitic and basaltic stones as a Quaternary age indicator, western United States: U.S. Geological Survey Professional Paper 1210, 56 p.
Crandell, D.R., 1987, Deposits of pre-1980 pyroclastic flows and lahars from Mount St. Helens, Washington: U.S. Geological Survey Professional Paper 1444, 91 p.
Crandell, D.R., and Miller, R.D., 1974, Quaternary stratigraphy and extent of glaciation in the Mount Rainier region, Washington: U.S. Geological Survey Professional Paper 847, 59 p.
Cummings, M.L., Pollock, J.M., Thompson, G.D., and Bull, M.K. 1990, Stratigraphic development and hydrothermal activity in the central western Cascade Range, Oregon: Journal of Geophysical Research, v. 95, p. 19,601–19,610.
Dethier, D.P., 1988, The soil chronosequence along the Cowlitz River, Washington: U.S. Geological Survey Bulletin 1590-F, p. F1–F47.
Doh, S.-J., and Steele, W.K., 1983, The late Pleistocene geomagnetic field as recorded by sediments from Fargher Lake, Washington, U.S.A.: Earth and Planetary Science Letters, v. 63, p. 385–398.
Duncan, R.A., and Kulm, L.D., 1989, Plate tectonic evolution of the Cascades arc-subduction complex, *in* Winterer, E.L., Hussong, D.M., and Decker, R.W., eds., The eastern Pacific Ocean and Hawaii: Boulder, Colo., Geological Society of America, The geology of North America, v. N, p. 413–438.
Evarts, R.C., 2001, Geologic map of the Silver Lake quadrangle, Cowlitz County, Washington: U.S. Geological Survey Miscellaneous Field Studies Map MF-2371, scale 1:24,000, with 37-p. pamphlet [Available on the World Wide Web at http://geopubs.wr.usgs.gov/map-mf/mf2371/].
Evarts, R.C., 2002, Geologic map of the Deer Island quadrangle, Columbia County, Oregon and Cowlitz County, Washington: U.S. Geological Survey Miscellaneous Field Studies Map MF-2392, scale 1:24,000, with 33-p. pamphlet [Available on the World Wide Web at http://geopubs.wr.usgs.gov/map-mf/mf2392/].
Evarts, R.C., 2004, Geologic map of the Woodland quadrangle, Clark and Cowlitz Counties, Washington: U.S. Geological Survey Scientific Investigations Map 2827, scale 1:24,000, with 38-p. pamphlet [Available on the World Wide Web at http://pubs.usgs.gov/sim/2004/2827].
Evarts, R.C., and Ashley, R.P., 1990a, Preliminary geologic map of the Cougar quadrangle, Cowlitz and Clark Counties, Washington: U.S. Geological Survey Open-File Report 90-631, scale 1:24,000, with 40-p. pamphlet.
Evarts, R.C., and Ashley, R.P., 1990b, Preliminary geologic map of the Goat Mountain quadrangle, Cowlitz County, Washington: U.S. Geological Survey Open-File Report 90-632, scale 1:24,000, with 47-p. pamphlet.
Evarts, R.C., and Ashley, R.P., 1991, Preliminary geologic map of the Lakeview Peak quadrangle, Cowlitz County, Washington: U.S. Geological Survey Open-File Report 91-289, scale 1:24,000, with 35-p. pamphlet.

Evarts, R.C., and Ashley, R.P., 1992, Preliminary geologic map of the Elk Mountain quadrangle, Cowlitz County, Washington: U.S. Geological Survey Open-File Report 92-362, scale 1:24,000, with 44-p. pamphlet.

Evarts, R.C., and Ashley, R.P., 1993, Geologic map of the Spirit Lake East quadrangle, Skamania County, Washington: U.S. Geological Survey Geologic Quadrangle Map GQ-1679, scale 1:24,000, with 12-p. pamphlet.

Evarts, R.C., Ashley, R.P., and Smith, J.G., 1987, Geology of the Mount St. Helens area—record of discontinuous volcanic and plutonic activity in the Cascade arc of southern Washington: Journal of Geophysical Research, v. 92, p. 10,155–10,169.

Evarts, R.C., and Bishop, K.R., 1994, Chemical data for Tertiary volcanic and intrusive rocks of the Spirit Lake 15-minute quadrangle, southern Washington Cascade Range: U.S. Geological Survey Open-File Report 93-686, 24 p.

Evarts, R.C., Clynne, M.A., Fleck, R.J., Lanphere, M.A., Calvert, A.T., and Sarna-Wojcicki, A.M., 2003, The antiquity of Mount St. Helens and age of the Hayden Creek Drift [abs.]: Geological Society of America Abstracts with program, v. 35, no. 6, p. 80.

Evarts, R.C., and Swanson, D.A., 1994, Geologic transect across the Tertiary Cascade Range, southern Washington, *in* Swanson, D.A., Haugerud, R.A., eds., Geologic field trips in the Pacific Northwest, 1994 Geological Society of America Meeting: Seattle, University of Washington Department of Geological Sciences, v. 2, p. 2H1–2H31.

Fiksdal, A.J., 1975, Slope stability of Clark County, Washington: Washington Division of Geology and Earth Resources Open-File Report 75-10, scale 1:62,500, with 4-p. pamphlet.

Fiske, R.S., Hopson, C.A., and Waters, A.C., 1963, Geology of Mount Rainier National Park, Washington: U.S. Geological Survey Professional Paper 444, 93 p.

Gill, J.B., 1981, Orogenic andesites and plate tectonics: New York, Springer-Verlag, 390 p.

Grant, A.R., 1969, Chemical and physical controls for base metal deposition in the Cascade Range of Washington: Washington Division of Mines and Geology Bulletin 58, 107 p.

Grigg, L.D., and Whitlock, C., 2002, Patterns and causes of millennial-scale climate change in the Pacific Northwest during Marine Isotope stages 2 and 3: Quaternary Science Reviews, v. 21, p. 2067–2083.

Hagstrum, J.T., Swanson, D.A., and Evarts, R.C., 1999, Paleomagnetism of an east-west transect across the Cascade arc in southern Washington—implications for regional tectonism: Journal of Geophysical Research, v. 104, p. 12,853–12,864.

Heusser, C.J., and Heusser, L.E., 1980, Sequence of pumiceous tephra layers and the late Quaternary environmental record near Mount St. Helens: Science, v. 210, p. 1007–1009.

Hodge, E.T., 1938, Geology of the lower Columbia River: Geological Society of America Bulletin, v. 49, p. 836–929.

Hollister, V.F., 1979, Porphyry copper-type deposits of the Cascade volcanic arc, Washington: Mineral Science and Engineering, v. 11, p. 22–35.

Howard, K.A., 2002, Geologic map of the Battle Ground 7.5-minute quadrangle, Clark County, Washington: U.S. Geological Survey Miscellaneous Field Studies Map MF-2395, scale 1:24,000, with 18-p. pamphlet [Available on the World Wide Web at http://geopubs.wr.usgs.gov/map-mf/mf2395/].

Johnson, D.M., Hooper, P.R., and Conrey, R.M., 1999, XRF analysis of rocks and minerals for major and trace elements on a single low dilution Li-tetraborate fused bead: Advances in X-ray Analysis, v. 41, p. 843–867.

Johnson, R.G., and King, B.-S., 1987, Energy-dispersive X-ray fluorescence spectrometry, *in* Baedecker, P.A., ed., Methods for geochemical analysis: U.S. Geological Survey Bulletin 1770, p. F1–F5.

King, B.-S., and Lindsay, J., 1990, Determination of 12 selected trace elements in geological materials by energy-dispersive X-ray fluorescence spectroscopy, *in* Arbogast, B.F., ed., Quality assurance manual for the Branch of Geochemistry, U.S. Geological Survey: U.S. Geological Survey Open-File Report 90-668, p. 161–165.

Le Maitre, R.W., 2002, Igneous rocks—a classification and glossary of terms, 2d ed.: Cambridge University Press, 236 p.

Liberty, L.M., Hemphill-Haley, M.A., and Madin, I.P., 2003, The Portland Hills Fault—uncovering a hidden fault in Portland, Oregon using high-resolution geophysical methods: Tectonophysics, v. 368, p. 89–103.

Lipman, P.W., 1984, The roots of ash flow caldera in western North America—windows into the tops of granitic batholiths: Journal of Geophysical Research, v. 89, p. 8801–8841.

Lipman, P.W., 1997, Subsidence of ash-flow calderas—relation to caldera size and magma-chamber geometry: Bulletin of Volcanology, v. 59, p. 198–218.

Livingston, V.E., Jr., 1966, Geology and mineral resources of Kelso-Cathlamet area, Cowlitz and Wahkiakum Counties, Washington: Washington Division of Mines and Geology Bulletin 54, 110 p.

Mabey, M.A., and Madin, I.P., 1995, Downhole and seismic cone penetrometer shear-wave velocity measurements for the Portland metropolitan area, 1993 and 1994: Oregon Department of Geology and Mineral Industries Open-File Report O-95-7, 69 p.

Madin, I.P, and Wang, Z., 1999, Relative earthquake hazard maps for selected urban areas in western Oregon—Dallas, Hood River, McMinnville-Dayton-Lafayette, Monmouth-Independence, Newberg-Dundee, Saint Helens-Columbia City-Scappoose, Sandy, Sheridan-Williamina: Oregon Department of Geology and Mineral Industries Interpretative Map Series IMS-7, scale 1:24,000, with 24-p. pamphlet.

Major, J.J., and Scott, K.M., 1988, Volcaniclastic sedimentation in the Lewis River valley, Mount St. Helens, Washington—processes, extent, and hazards: U.S. Geological Survey Bulletin 1383-D, 38 p.

Martinson, D.G., Pisias, N.G., Hayes, J.D., Imbrie, J., Moore, T.C., Jr., and Shackleton, N.J., 1987, Age dating and orbital theory of the ice ages—development of a high-resolution 0 to 300,000-year chronostratigraphy: Quaternary Research, v. 27, p. 1–29.

McDonald, E.V., and Busacca, A.J., 1988, Record of pre-late Wisconsin giant floods in the Channeled Scabland interpreted from loess deposits: Geology, v. 16, p. 728–731.

Miall, A.D., 1977, A review of the braided river depositional environment: Earth-Science Reviews, v. 13, p. 1–62.

Miall, A.D., 1996, The geology of fluvial deposits—sedimentary facies, basin analysis, and petroleum geology: Berlin, Springer, 582 p.

Miyashiro, A., 1974, Volcanic rocks series in island arcs and active continental margins: American Journal of Science, v. 274, p. 321–355.

Moen, W.S., 1977, St. Helens and Washougal Mining Districts of the southern Cascades of Washington: Washington Division of Geology and Earth Resources Information Circular No. 60, 71 p.

Mullineaux, D.R., 1996, Pre-1980 tephra-fall deposits erupted from Mount St. Helens: U.S. Geological Survey Professional Paper 1563, 99 p.

Mundorff, M.J., 1964, Geology and ground-water conditions of Clark County, Washington, with a description of a major alluvial aquifer along the Columbia River: U.S. Geological Survey Water-Supply Paper 1600, 268 p., scale 1:48,000.

Mundorff, M.J., 1984, Glaciation in the lower Lewis River basin, southwestern Cascade Range, Washington: Northwest Science, v. 58, p. 269–281.

Nakamura, K., 1977, Volcanoes as possible indicators of tectonic stress orientation—principles and proposal: Journal of Volcanological and Geothermal Research, v. 2, p. 1–16.

O'Connor, J.E., and Baker, V.R., 1992, Magnitudes and implications of peak discharges from glacial Lake Missoula: Geological Society of America Bulletin, v. 104, p. 267–279.

Orton, G.J., 1996, Volcanic environments, *in* Reading, H.G., ed., Sedimentary environments—processes, facies and stratigraphy (3d ed.): Oxford, Blackwell Science, Ltd., p. 485–567.

Pezzopane, S.K., and Weldon, R.J., II, 1993, Tectonic role of active faulting in central Oregon: Tectonics, v. 12, p. 1140–1169.

Phillips, W.M, 1987a, comp., Geologic map of the Vancouver quadrangle, Washington: Washington Division of Geology and Earth Resources Open-File Report 87-10, scale 1:100,000, with 27-p. pamphlet.

Phillips, W.M, 1987b, comp., Geologic map of the Mount St. Helens quadrangle, Washington: Washington Division of Geology and Earth Resources Open-File Report 87-4, scale 1:100,000, with 59-p. pamphlet.

Rigg, G.B., 1958, Peat resources of Washington: Washington Division of Mines and Geology Bulletin 44, 272 p.

Rust, B.R., 1978, Depositional models for braided alluvium, *in* Miall, A.D., ed., Fluvial sedimentology: Canadian Society of Petroleum Geologists Memoir 5, p. 605–625.

Smith, G.A., 1986, Coarse-grained nonmarine volcaniclastic sediment—terminology and depositional processes: Geological Society of America Bulletin, v. 97, p. 1–10.

Smith, J.G., 1993, Geologic map of upper Eocene to Holocene volcanic and related rocks in the Cascade Range, Washington: U.S. Geological Survey Miscellaneous Investigation Series Map I-2005, scale 1:500,000.

Swanson, R.D., McFarland, W.D., Gonthier, J.B., and Wilkinson, J.M., 1993, A description of hydrogeologic units in the Portland Basin, Oregon and Washington: U.S. Geological Survey Water-Resources Investigations Report 90-4196, 56 p., scale 1:100,000.

Taggart, J.E., Jr., Lindsay, J.R., Scott, B.A., Vivit, D.V., Bartel, A.J., and Stewart, K.C., 1987, Analysis of geological materials by wavelength-dispersive X-ray fluorescence spectrometry, *in* Baedecker, P.A., ed., Methods for geochemical analysis: U.S. Geological Survey Bulletin 1770, p. E1–E19.

Tilford, N.R., and Sullivan, J.G., 1981, Lewis River hydroelectric developments, *in* Field Trip Guidebook, Engineering geology of the Pacific Northwest: Association of Engineering Geologists Annual Meeting, 1981, Portland, Oreg., p. 156–185.

Tolan T.L., and Beeson, M.H., 1984, Intracanyon flows of the Columbia River Basalt group in the lower Columbia River Gorge and their relationship to the Troutdale Formation: Geological Society of America Bulletin, v. 95, p. 463–477.

Trimble, D.E., 1963, Geology of Portland, Oregon and adjacent areas: U.S. Geological Survey Bulletin 1119, 119 p., scale 1:62,500.

Verplanck, E.P., and Duncan, R.A., 1987, Temporal variations in plate convergence and eruption rates in the western Cascades, Oregon: Tectonics, v. 6, p. 197–209.

Vessell, R.K., and Davies, D.K., 1981, Nonmarine sedimentation in an active fore arc basin, *in* Ethridge, F.G., and Flores, R.M., eds., Recent and ancient nonmarine depositional environments—models for exploration: Society of Economic Paleontologists and Mineralogists Special Publication 31, p. 31–45.

Waitt, R.B., Jr., 1985, Case for periodic, colossal jökulhlaups from Pleistocene glacial Lake Missoula: Geological Society of America, v. 96, p. 1271–1286.

Waitt, R.B., Jr., 1994, Scores of gigantic, successively smaller Lake Missoula floods through channeled scabland and Columbia valley, *in* Swanson, D.A., and Haugerud, R.A., eds., Geologic field trips in the Pacific Northwest: Seattle, University of Washington Department of Geological Sciences, p. 1K1–1K88.

Waitt, R.B., Jr., 1996, Numerous colossal Missoula Floods through Columbia Gorge and Portland-Vancouver basin [abs.], Geological Society of America Abstracts with Program, v. 28, no. 5, p. 120–121.

Walsh, T.J., Korosec, M.A., Phillips, W.M., Logan, R.L., and Schasse, H.W., 1987, Geologic map of Washington—southwest quadrant: Washington Division of Geology and Earth Resources Map GM-34, scale 1:250,000.

Warne, A.G., and Stanley, D.J., 1995, Sea-level changes as critical factor in development of basin margin sequences—new evidence from late Quaternary record: Journal of Coastal Research Special Issue 17, p. 231–240.

Wegmann, K.W., and Walsh, T.J., 2001, Landslide hazards mapping in Cowlitz County—a progress report: Washington Geology, v. 29, no. 1/2, p. 30–33.

Wells, R.E., 1981, Geologic map of the eastern Willapa Hills, Cowlitz, Lewis, Pacific, and Wahkiakum Counties, Washington: U.S. Geological Survey Open-File Report 81-674, scale 1:62,500.

Wells, R.E., 1989, Mechanisms of Cenozoic tectonic rotation, Pacific Northwest convergent margin, U.S.A., *in* Kissel, C., and Laj, C., eds., Paleomagnetic rotations and continental deformation: Dordrecht, Kluwer Academic Publishers, p. 313–325.

Wells, R.E., 1990, Paleomagnetic rotations and the Cenozoic tectonics of the Cascade arc, Washington, Oregon, and California: Journal of Geophysical Research, v. 95, p. 19,409–19,417.

Wells, R.E., and Coe, R.S., 1985, Paleomagnetism and geology of Eocene volcanic rocks of southwest Washington, implications for mechanisms of tectonic rotation: Journal of Geophysical Research, v. 90, p. 1925–1947.

Wells, R.E., Engebretson, D.C., Snavely, P.D., Jr., and Coe, R.S., 1984, Cenozoic plate motions and the volcano-tectonic evolution of western Oregon and Washington: Tectonics, v. 3, p. 275–294.

Wells, R.E., Weaver, C.S., and Blakely, R.J., 1998, Fore-arc migration in Cascadia and its neotectonic significance: Geology, v. 26, p. 759–762.

Whitlock, C., Sarna-Wojcicki, A.M., Bartlein, P.J., and Nickmann, R.J., 2000, Environmental history and tephrostratigraphy at Carp Lake, southwestern Columbia Basin, USA: Paleogeography, Paleoclimatology, Paleoecology, v. 155, p. 7–29.

Wilkinson, W.D., Lowry, W.D., and Baldwin, E.M., 1946, Geology of the St. Helens quadrangle, Oregon: Oregon Department of Geology and Mineral Industries Bulletin 31, 39 p., scale 1:62,500.

Williams, H., and McBirney, A.R., 1979, Volcanology: San Francisco, Freeman, Cooper and Co., 397 p.

Williams, I., 1933, Geology of Ariel dam site [abs.]: Geological Society of America Bulletin, v. 44, p. 157–158.

Wise, W.S., 1970, Cenozoic volcanism in the Cascade Mountains of southern Washington: Washington Division of Mines and Geology Bulletin 60, 45 p.

Wolfe, J.A., 1978, A paleobotanical interpretation of Tertiary climates in the Northern Hemisphere: American Scientist, v. 66, p. 694–703.

Wolfe, J.A., and Hopkins, D.M., 1967, Climatic changes recorded by Tertiary land floras in northwestern North America, *in* Hatai, Kotora, ed., Tertiary correlations and climatic changes in the Pacific: Sendai, Japan, Sendai Printing and Publishing, p. 67–76.

Wong, I.G., Hemphill-Haley, A., Liberty, L.M., and Madin, I.P., 2001, The Portland Hills Fault—an earthquake generator or just another old fault?: Oregon Geology, v. 63, p. 39–50.

Yeats, R.S., Graven, E.P., Werner, K.S., Goldfinger, Chris, and Popowski, T.A., 1996, Tectonics of the Willamette Valley, Oregon, *in* Rogers, A.M., Walsh, T.J., Kockelman, W.J., and Priest, G.R., eds., Assessing earthquake hazards and reducing risk in the Pacific Northwest: U.S. Geological Survey Professional Paper 1650, v. 1, p. 183–222.

Yelin, T.S., and Patton, H.J., 1991, Seismotectonics of the Portland, Oregon, region: Seismological Society of America Bulletin, v. 81, p. 109–130.

Zuffa, G.G., Normark, W.R., Serra, F., and Brunner, C.A., 2000, Turbidite megabeds in an oceanic rift valley recording jökulhlaups of late Pleistocene glacial lakes of the western United States: Journal of Geology, v. 108, p. 253–274.

**Table 1.** Chemical analyses and modes of volcanic and intrusive rocks, Ariel 7.5' quadrangle

[X-ray fluorescence analyses. Rock-type names assigned in accordance with IUGS system (Le Maitre, 2002) applied to recalculated analyses. LOI, loss on ignition. Mg#, atomic ratio 100Mg/(Mg+$Fe^{2+}$) with $Fe^{2+}$ set to 0.85x $Fe^{total}$. Modal analyses, secondary minerals counted as primary mineral replaced. -, not present; ---, no data; interstit, interstitial. Analyses by D.F. Siems at U.S. Geological Survey, Lakewood, Colo., using methods described in Taggart and others (1987), Johnson and King (1987), and King and Lindsay (1990). *, analyses by D.M. Johnson at GeoAnalytical Laboratory of Washington State University using methods described in Johnson and others (1999)]

| Map No. | 1 | 2 | 3 | 4 | 5 | 6 | 7 | 8 | 9 |
|---|---|---|---|---|---|---|---|---|---|
| Field sample No. | 99LC-Q395A* | 99LC-Q392A* | 99LC-Q384B* | 01LC-Q470A* | 99LC-Q326B* | 00LC-Q414* | 98LC-Q166 | 00LC-Q403* | 00LC-Q445* |
| Latitude (N) | 45°55.62' | 45°55.20' | 45°55.26' | 45°52.56' | 45°57.50' | 45°57.24' | 45°54.30' | 45°59.28' | 45°56.64' |
| Longitude (W) | 122°33.06' | 122°35.52' | 122°35.46' | 122°36.54' | 122°35.46' | 122°35.82' | 122°31.08' | 122°37.20' | 122°36.12' |
| Map unit | Tob | Tob | Tob | Tba | Tba | Tba | Tba | Tba | Tba |
| Rock type | Basalt | Basalt | Basaltic andesite | Basalt | Basaltic andesite | Basaltic andesite | Basaltic andesite | Basaltic andesite | Basaltic andesite |
| Analyses as reported (wt. percent) | | | | | | | | | |
| $SiO_2$ | 48.45 | 50.90 | 52.97 | 50.75 | 52.34 | 52.85 | 51.66 | 53.23 | 53.43 |
| $TiO_2$ | 2.51 | 1.85 | 1.05 | 1.94 | 1.09 | 0.89 | 1.18 | 0.92 | 0.91 |
| $Al_2O_3$ | 16.60 | 16.32 | 17.52 | 16.49 | 17.41 | 19.39 | 17.23 | 19.57 | 19.19 |
| $Fe_2O_3$ | --- | --- | --- | --- | --- | --- | 9.54 | --- | --- |
| FeO | 11.80 | 10.26 | 8.54 | 9.80 | 8.38 | 7.43 | --- | 7.12 | 7.24 |
| MnO | 0.26 | 0.18 | 0.16 | 0.19 | 0.16 | 0.16 | 0.15 | 0.14 | 0.15 |
| MgO | 5.90 | 6.64 | 6.77 | 6.17 | 6.48 | 5.37 | 5.64 | 5.42 | 4.91 |
| CaO | 10.05 | 9.44 | 9.22 | 9.73 | 9.77 | 9.87 | 9.48 | 10.14 | 10.15 |
| $Na_2O$ | 2.79 | 2.98 | 3.01 | 2.98 | 2.73 | 2.82 | 2.79 | 2.57 | 2.85 |
| $K_2O$ | 0.17 | 0.33 | 0.35 | 0.47 | 0.63 | 0.91 | 0.48 | 0.97 | 0.91 |
| $P_2O_5$ | 0.42 | 0.31 | 0.17 | 0.39 | 0.16 | 0.14 | 0.18 | 0.15 | 0.15 |
| LOI | --- | --- | --- | --- | --- | --- | 1.25 | --- | --- |
| Total | 98.94 | 99.21 | 99.75 | 98.91 | 99.15 | 99.83 | 99.57 | 100.22 | 99.90 |
| Analyses recalculated volatile-free and normalized to 100% with all Fe as FeO (wt. percent) | | | | | | | | | |
| $SiO_2$ | 48.97 | 51.30 | 53.10 | 51.31 | 52.79 | 52.94 | 52.98 | 53.11 | 53.48 |
| $TiO_2$ | 2.53 | 1.87 | 1.05 | 1.96 | 1.10 | 0.89 | 1.21 | 0.92 | 0.91 |
| $Al_2O_3$ | 16.78 | 16.45 | 17.56 | 16.67 | 17.56 | 19.42 | 17.67 | 19.53 | 19.21 |
| FeO* | 11.92 | 10.34 | 8.56 | 9.90 | 8.45 | 7.45 | 8.95 | 7.10 | 7.25 |
| MnO | 0.26 | 0.18 | 0.16 | 0.19 | 0.16 | 0.16 | 0.15 | 0.14 | 0.15 |
| MgO | 5.96 | 6.69 | 6.79 | 6.24 | 6.54 | 5.38 | 5.78 | 5.41 | 4.91 |
| CaO | 10.16 | 9.51 | 9.24 | 9.84 | 9.85 | 9.89 | 9.72 | 10.12 | 10.16 |
| $Na_2O$ | 2.82 | 3.00 | 3.02 | 3.01 | 2.75 | 2.82 | 2.86 | 2.56 | 2.85 |
| $K_2O$ | 0.17 | 0.33 | 0.35 | 0.48 | 0.64 | 0.91 | 0.49 | 0.97 | 0.91 |
| $P_2O_5$ | 0.42 | 0.31 | 0.17 | 0.40 | 0.16 | 0.1 | 0.18 | 0.1 | 0.15 |
| Mg# | 51.2 | 57.6 | 62.4 | 56.9 | 61.9 | 60.2 | 57.5 | 61.5 | 58.7 |
| Modes (volume percent) | | | | | | | | | |
| Plagioclase | 0.5 | - | - | 0.6 | 2.4 | 17.6 | 18.6 | 29.2 | 23.3 |
| Clinopyroxene | - | - | - | - | 2.4 | 2.5 | 1.0 | 3.2 | 6.6 |
| Orthopyroxene | - | - | - | - | - | - | 1.0 | 0.8 | - |
| Olivine | 2.6 | 4.9 | 2.3 | 0.9 | 1.6 | 2.5 | trace | 4.5 | 5.1 |
| Fe-Ti Oxide | - | - | - | trace | - | - | - | - | - |
| Hornblende | - | - | - | - | - | - | - | - | - |
| Quartz | - | - | - | - | - | - | - | - | - |
| K-feldspar | - | - | - | - | - | - | - | - | - |
| Other | - | - | - | - | - | - | - | - | - |
| Groundmass | 96.9 | 95.1 | 97.7 | 98.5 | 93.6 | 77.4 | 79.4 | 62.3 | 65.0 |
| No. points counted | 753 | 760 | 780 | 800 | 778 | 765 | 780 | 785 | 800 |
| Texture (rock/ groundmass) | seriate/ intergranular | seriate/ intergranular | porphyritic/ trachytic | seriate/ trachytic | seriate/ intergranular | seriate/ intergranular | seriate/ intersertal | glomerophyric/ intergranular | glomerophyric/ intergranular |
| Trace element analyses (ppm) | | | | | | | | | |
| Ba | 112 | 140 | 107 | 159 | 163 | 132 | 156 | 129 | 147 |
| Rb | 0 | 5 | 4 | 7 | 6 | 12 | 14 | 8 | 11 |
| Sr | 417 | 368 | 349 | 372 | 482 | 482 | 338 | 492 | 507 |
| Y | 35 | 25 | 19 | 31 | 22 | 16 | 21 | 16 | 15 |
| Zr | 197 | 152 | 97 | 199 | 101 | 95 | 112 | 99 | 96 |
| Nb | 18.4 | 14.1 | 7.5 | 20.3 | 6.3 | 3.7 | 11 | 4.8 | 6 |
| Ni | 88 | 119 | 117 | 94 | 48 | 30 | 48 | 26 | 32 |
| Cu | 193 | 137 | 101 | 171 | 92 | 163 | 159 | 87 | 49 |
| Zn | 113 | 98 | 76 | 100 | 76 | 57 | 79 | 60 | 55 |
| Cr | 156 | 205 | 224 | 140 | 111 | 62 | --- | 57 | 70 |

**Table 1.** Chemical analyses of volcanic and intrusive rocks, Ariel 7.5' quadrangle—Continued

| Map No. | 10 | 11 | 12 | 13 | 14 | 15 | 16 | 17 | 18 |
|---|---|---|---|---|---|---|---|---|---|
| Field sample No. | 98LC-Q290 | 00LC-Q456* | 97LC-Q15 | 01LC-Q468* | 97LC-Q130 | 99LC-Q326A* | 99LC-Q340* | 00LC-Q418* | 00LC-Q416A* |
| Latitude (N) | 45°59.40' | 45°56.04' | 45°59.76' | 45°59.94' | 45°57.84' | 45°57.52' | 45°59.94' | 45°56.94' | 45°58.14' |
| Longitude (W) | 122°30.18' | 122°33.24' | 122°37.44' | 122°34.02' | 122°35.10' | 122°35.59 | 122°30.96' | 122°33.30' | 122°32.10 |
| Map unit | Tba | Tba | Tba | Ta | Tba | Tba | Tba | Tba | Ta |
| Rock type | Basaltic andesite | Basaltic andesite | Basaltic andesite | Basaltic andesite | Basaltic andesite | Basaltic andesite | Basaltic andesite | Basaltic andesite | Basaltic andesite |
| Analyses as reported (wt. percent) | | | | | | | | | |
| $SiO_2$ | 52.26 | 53.57 | 52.29 | 53.21 | 52.95 | 53.95 | 54.69 | 54.75 | 54.54 |
| $TiO_2$ | 1.37 | 1.42 | 1.16 | 1.42 | 1.38 | 1.01 | 1.11 | 0.96 | 1.15 |
| $Al_2O_3$ | 16.64 | 17.87 | 17.49 | 17.29 | 17.37 | 18.00 | 18.30 | 18.70 | 16.98 |
| $Fe_2O_3$ | 9.54 | --- | 8.97 | --- | 9.79 | --- | --- | --- | --- |
| FeO | --- | 8.33 | --- | 8.48 | --- | 7.58 | 7.51 | 7.48 | 8.29 |
| MnO | 0.15 | 0.15 | 0.14 | 0.14 | 0.28 | 0.16 | 0.13 | 0.13 | 0.15 |
| MgO | 5.19 | 4.49 | 5.48 | 5.05 | 3.80 | 5.16 | 4.59 | 4.64 | 5.65 |
| CaO | 9.17 | 10.07 | 9.29 | 8.62 | 8.59 | 9.34 | 9.02 | 8.77 | 9.00 |
| $Na_2O$ | 3.13 | 3.17 | 2.88 | 3.01 | 3.36 | 3.20 | 3.53 | 3.40 | 2.98 |
| $K_2O$ | 0.78 | 0.59 | 0.36 | 0.70 | 0.73 | 0.52 | 0.77 | 0.92 | 0.49 |
| $P_2O_5$ | 0.27 | 0.29 | 0.20 | 0.22 | 0.22 | 0.20 | 0.18 | 0.17 | 0.24 |
| LOI | 1.01 | --- | 1.87 | --- | 1.24 | --- | --- | --- | --- |
| Total | 99.50 | 99.94 | 100.14 | 98.14 | 99.71 | 99.12 | 99.83 | 99.92 | 99.47 |
| Analyses recalculated volatile-free and normalized to 100% with all Fe as FeO (wt. percent) | | | | | | | | | |
| $SiO_2$ | 53.51 | 53.60 | 53.63 | 54.22 | 54.24 | 54.43 | 54.78 | 54.79 | 54.83 |
| $TiO_2$ | 1.40 | 1.42 | 1.19 | 1.44 | 1.42 | 1.02 | 1.11 | 0.96 | 1.16 |
| $Al_2O_3$ | 17.03 | 17.88 | 17.94 | 17.62 | 17.80 | 18.16 | 18.33 | 18.72 | 17.07 |
| FeO* | 8.92 | 8.33 | 8.42 | 8.64 | 9.17 | 7.65 | 7.52 | 7.48 | 8.33 |
| MnO | 0.15 | 0.15 | 0.15 | 0.14 | 0.29 | 0.16 | 0.13 | 0.13 | 0.15 |
| MgO | 5.31 | 4.49 | 5.62 | 5.15 | 3.89 | 5.21 | 4.60 | 4.64 | 5.68 |
| CaO | 9.39 | 10.08 | 9.53 | 8.78 | 8.79 | 9.42 | 9.04 | 8.78 | 9.05 |
| $Na_2O$ | 3.20 | 3.17 | 2.95 | 3.07 | 3.44 | 3.23 | 3.54 | 3.40 | 3.00 |
| $K_2O$ | 0.80 | 0.59 | 0.37 | 0.71 | 0.75 | 0.52 | 0.77 | 0.92 | 0.49 |
| $P_2O_5$ | 0.28 | 0.29 | 0.21 | 0.22 | 0.23 | 0.20 | 0.18 | 0.17 | 0.24 |
| Mg# | 55.5 | 53.1 | 58.3 | 55.5 | 47.1 | 58.8 | 56.2 | 56.6 | 58.9 |
| Modes (volume percent) | | | | | | | | | |
| Plagioclase | 0.8 | 16.5 | 10.1 | 29.6 | 20.7 | 17.8 | 14.4 | 20.3 | 23.4 |
| Clinopyroxene | 0.1 | 0.4 | 1.5 | 0.1 | - | 2.0 | 4.1 | 0.1 | 3.3 |
| Orthopyroxene | - | - | 0.9 | 2.6 | 1.9 | - | - | - | 4.3 |
| Olivine | 0.6 | 0.4 | 3.1 | 1.0 | - | 2.4 | 1.4 | 3.5 | 2.8 |
| Fe-Ti Oxide | - | - | - | trace | - | 0.1 | trace | - | 0.1 |
| Hornblende | - | - | - | - | - | - | - | - | - |
| Quartz | - | - | - | - | - | - | - | - | - |
| K-feldspar | - | - | - | - | - | - | - | - | - |
| Other | - | - | - | - | - | - | - | - | - |
| Groundmass | 98.5 | 82.7 | 84.4 | 66.7 | 77.4 | 77.7 | 80.1 | 76.1 | 66.1 |
| No. points counted | 810 | 814 | 797 | 808 | 700 | 785 | 800 | 800 | 812 |
| Texture (rock/ groundmass) | seriate/ intergranular | glomerophyric/ intergranular | seriate/ intergranular | seriate/ intergranular | seriate/ intergranular | seriate/ intergranular | seriate/ intergranular | seriate/ intergranular | porphyritic/ intergranular |
| Trace element analyses (ppm) | | | | | | | | | |
| Ba | 201 | 179 | 141 | 193 | 174 | 247 | 157 | 162 | 185 |
| Rb | 16 | 13 | <10 | 6 | 16 | 21 | 13 | 12 | 11 |
| Sr | 402 | 380 | 411 | 435 | 446 | 551 | 416 | 440 | 421 |
| Y | 21 | 24 | 18 | 24 | 16 | 22 | 18 | 18 | 22 |
| Zr | 145 | 155 | 120 | 153 | 120 | 123 | 118 | 125 | 159 |
| Nb | 14 | 13.2 | 12 | 11.3 | 12 | 7.8 | 9.3 | 7.8 | 10.3 |
| Ni | 62 | 30 | --- | 51 | --- | 48 | 29 | 47 | 71 |
| Cu | 101 | 107 | --- | 149 | --- | 114 | 96 | 94 | 78 |
| Zn | 80 | 74 | --- | 81 | --- | 72 | 71 | 67 | 75 |
| Cr | --- | 87 | --- | 60 | --- | 71 | 60 | 64 | 111 |

**Table 1.** Chemical analyses of volcanic and intrusive rocks, Ariel 7.5' quadrangle—Continued

| Map No. | 19 | 20 | 21 | 22 | 23 | 24 | 25 | 26 | 27 |
|---|---|---|---|---|---|---|---|---|---|
| Field sample No. | 97LC-Q02B | 98LC-Q261 | 99LC-Q392C* | 99LC-Q377* | 99LC-Q357* | 01LC-Q466* | 99LC-Q380* | 00LC-Q462A* | 97LC-Q121A |
| Latitude (N)<br>Longitude (W) | 45°57.36'<br>122°34.80' | 45°59.22'<br>122°30.96' | 45°55.14'<br>122°35.22' | 45°54.78'<br>122°31.20' | 45°59.46'<br>122°36.36' | 45°52.80'<br>122°30.12' | 45°55.56'<br>122°31.08' | 45°57.31'<br>122°33.41' | 45°59.64'<br>122°35.46' |
| Map unit | Tba | Tba | Tba | Tba | Tba | Tba | Tba | Tba | Tdpc† |
| Rock type | Basaltic andesite | Basaltic andesite | Basaltic andesite | Basaltic andesite | Basaltic andesite | Basaltic andesite | Basaltic andesite | Basaltic andesite | Basaltic andesite |
| Analyses as reported (wt. percent) | | | | | | | | | |
| $SiO_2$ | 53.83 | 53.52 | 54.67 | 55.03 | 55.44 | 54.95 | 55.66 | 56.01 | 55.06 |
| $TiO_2$ | 1.68 | 1.12 | 0.99 | 1.20 | 1.10 | 1.17 | 1.67 | 1.24 | 1.17 |
| $Al_2O_3$ | 15.95 | 17.23 | 18.01 | 17.08 | 17.41 | 19.23 | 16.57 | 17.92 | 17.56 |
| $Fe_2O_3$ | 10.32 | 8.86 | --- | --- | --- | --- | --- | --- | 8.24 |
| FeO | --- | --- | 7.52 | 7.94 | 7.95 | 7.39 | 8.98 | 7.91 | --- |
| MnO | 0.16 | 0.14 | 0.23 | 0.15 | 0.14 | 0.15 | 0.14 | 0.15 | 0.14 |
| MgO | 4.34 | 4.36 | 4.62 | 5.02 | 4.25 | 2.72 | 3.72 | 3.66 | 3.70 |
| CaO | 7.66 | 9.08 | 9.38 | 8.67 | 8.79 | 8.66 | 7.72 | 8.15 | 8.10 |
| $Na_2O$ | 3.49 | 3.01 | 3.22 | 3.36 | 3.41 | 3.69 | 3.69 | 3.78 | 3.49 |
| $K_2O$ | 1.32 | 0.72 | 0.54 | 0.89 | 1.04 | 0.53 | 1.08 | 0.89 | 1.00 |
| $P_2O_5$ | 0.37 | 0.20 | 0.16 | 0.21 | 0.20 | 0.18 | 0.30 | 0.16 | 0.22 |
| LOI | 0.59 | 1.15 | --- | --- | --- | --- | --- | --- | 1.23 |
| Total | 99.69 | 99.38 | 99.33 | 99.55 | 99.73 | 98.67 | 99.53 | 99.86 | 99.89 |
| Analyses recalculated volatile-free and normalized to 100% with all Fe as FeO (wt. percent) | | | | | | | | | |
| $SiO_2$ | 54.85 | 54.90 | 55.04 | 55.28 | 55.59 | 55.69 | 55.92 | 56.09 | 56.22 |
| $TiO_2$ | 1.71 | 1.15 | 1.00 | 1.21 | 1.10 | 1.18 | 1.68 | 1.24 | 1.19 |
| $Al_2O_3$ | 16.25 | 17.67 | 18.13 | 17.16 | 17.46 | 19.49 | 16.65 | 17.94 | 17.93 |
| FeO* | 9.54 | 8.32 | 7.57 | 7.97 | 7.97 | 7.49 | 9.02 | 7.92 | 7.67 |
| MnO | 0.17 | 0.15 | 0.23 | 0.15 | 0.14 | 0.16 | 0.14 | 0.15 | 0.14 |
| MgO | 4.42 | 4.48 | 4.65 | 5.04 | 4.26 | 2.76 | 3.74 | 3.67 | 3.78 |
| CaO | 7.80 | 9.31 | 9.44 | 8.71 | 8.81 | 8.78 | 7.76 | 8.16 | 8.27 |
| $Na_2O$ | 3.55 | 3.08 | 3.24 | 3.38 | 3.42 | 3.74 | 3.71 | 3.79 | 3.56 |
| $K_2O$ | 1.34 | 0.74 | 0.54 | 0.89 | 1.04 | 0.54 | 1.09 | 0.89 | 1.02 |
| $P_2O_5$ | 0.38 | 0.21 | 0.16 | 0.21 | 0.20 | 0.18 | 0.31 | 0.16 | 0.22 |
| Mg# | 49.3 | 53.0 | 56.3 | 57.0 | 52.9 | 43.6 | 46.5 | 49.3 | 50.8 |
| Modes (volume percent) | | | | | | | | | |
| Plagioclase | 2.1 | 22.0 | 9.7 | 40.6 | 8.4 | 25.9 | 6.9 | 7.5 | 17.7 |
| Clinopyroxene | 0.1 | 0.1 | 0.9 | 0.3 | 1.0 | 0.1 | 0.3 | 1.2 | 0.3 |
| Orthopyroxene | 0.2 | - | - | 4.2 | - | - | - | 0.4 | trace |
| Olivine | 0.1 | 0.9 | 5.2 | 1.2 | 0.5 | 0.5 | - | 2.3 | 0.1 |
| Fe-Ti Oxide | trace | trace | - | trace | - | 0.3 | - | 0.1 | - |
| Hornblende | - | - | - | - | - | - | - | - | - |
| Quartz | - | - | - | - | - | - | - | - | - |
| K-feldspar | - | - | - | - | - | - | - | - | - |
| Other | - | - | - | - | - | - | - | - | - |
| Groundmass | 97.5 | 77.0 | 84.2 | 53.7 | 90.1 | 73.2 | 92.8 | 88.5 | 81.9 |
| No. points counted | 778 | 810 | 802 | 814 | 790 | 792 | 800 | 800 | 650 |
| Texture (rock/ groundmass) | sparsely phyric/ intergranular | porphyritic/ intergranular | seriate/ intergranular | seriate/ intergranular | seriate/ intergranular | seriate/ intersertal | seriate/ intergranular | seriate/ trachytic | seriate/ intergranular |
| Trace element analyses (ppm) | | | | | | | | | |
| Ba | 288 | 165 | 128 | 183 | 187 | 159 | 203 | 184 | 166 |
| Rb | 25 | 12 | 19 | 21 | 17 | 11 | 22 | 16 | 15 |
| Sr | 434 | 371 | 350 | 294 | 394 | 348 | 301 | 405 | 387 |
| Y | 30 | 20 | 26 | 26 | 21 | 25 | 35 | 22 | 19 |
| Zr | 219 | 128 | 123 | 148 | 135 | 115 | 215 | 125 | 148 |
| Nb | 14.0 | 8 | 8.5 | 9.8 | 9.4 | 10.2 | 14.3 | 8.0 | 11 |
| Ni | --- | 31 | 69 | 30 | 13 | 3 | 15 | 23 | --- |
| Cu | --- | 114 | 82 | 73 | 120 | 122 | 325 | 90 | --- |
| Zn | --- | 70 | 73 | 79 | 70 | 81 | 91 | 70 | --- |
| Cr | --- | --- | 106 | 76 | 36 | 8 | 28 | 32 | --- |

† Sample from megablock in caldera fill.

**Table 1.** Chemical analyses of volcanic and intrusive rocks, Ariel 7.5' quadrangle—Continued

| Map No. | 28 | 29 | 30 | 31 | 32 | 33 | 34 | 35 | 36 |
|---|---|---|---|---|---|---|---|---|---|
| Field sample No. | 99LC-Q355B* | 99LC-Q394* | 98LC-Q260 | 98LC-Q209 | 99LC-Q360* | 98LC-Q249 | 98LC-Q167 | 00LC-Q437* | 98LC-Q219A |
| Latitude (N)<br>Longitude (W) | 45°59.70'<br>122°36.00' | 45°55.56'<br>122°30.60' | 45°59.94'<br>122°30.60' | 45°58.14'<br>122°31.02' | 45°59.22'<br>122°35.88' | 45°56.46'<br>122°30.42' | 45°56.88'<br>122°32.58' | 45°58.62'<br>122°30.18' | 45°59.15'<br>122°33.48' |
| Map unit | Tba | Tba | Tba | Ta | Tdpc† | Ta | Ta | Ta | Ta |
| Rock type | Basaltic andesite | Basaltic andesite | Basaltic andesite | Andesite | Andesite | Andesite | Andesite | Andesite | Andesite |
| Analyses as reported (wt. percent) | | | | | | | | | |
| $SiO_2$ | 56.05 | 56.72 | 55.36 | 55.73 | 58.64 | 57.68 | 58.82 | 59.85 | 58.76 |
| $TiO_2$ | 1.11 | 1.14 | 0.91 | 1.17 | 1.21 | 1.00 | 0.91 | 1.01 | 0.94 |
| $Al_2O_3$ | 17.05 | 17.12 | 18.08 | 17.04 | 16.30 | 16.60 | 17.03 | 15.95 | 16.47 |
| $Fe_2O_3$ | --- | --- | 6.95 | 8.13 | --- | 7.02 | 6.64 | --- | 6.80 |
| FeO | 7.86 | 7.09 | --- | --- | 7.84 | --- | --- | 6.71 | --- |
| MnO | 0.14 | 0.15 | 0.10 | 0.12 | 0.15 | 0.12 | 0.13 | 0.11 | 0.12 |
| MgO | 3.99 | 3.77 | 3.75 | 3.96 | 3.13 | 3.91 | 3.18 | 3.70 | 2.88 |
| CaO | 8.43 | 7.86 | 7.98 | 7.32 | 6.79 | 6.56 | 6.29 | 6.51 | 6.16 |
| $Na_2O$ | 3.42 | 3.86 | 3.56 | 3.43 | 4.06 | 3.57 | 3.80 | 3.62 | 3.80 |
| $K_2O$ | 1.03 | 1.47 | 0.84 | 1.00 | 1.23 | 1.20 | 1.31 | 1.44 | 1.15 |
| $P_2O_5$ | 0.20 | 0.38 | 0.18 | 0.20 | 0.23 | 0.21 | 0.16 | 0.22 | 0.25 |
| LOI | --- | --- | 1.85 | 1.23 | --- | 1.30 | 1.19 | --- | 1.76 |
| Total | 99.28 | 99.56 | 99.56 | 99.32 | 99.57 | 99.16 | 99.44 | 99.12 | 99.08 |
| Analyses recalculated volatile-free and normalized to 100% with all Fe as FeO (wt. percent) | | | | | | | | | |
| $SiO_2$ | 56.46 | 56.97 | 56.98 | 57.21 | 58.89 | 59.28 | 60.21 | 60.38 | 60.70 |
| $TiO_2$ | 1.12 | 1.15 | 0.93 | 1.20 | 1.22 | 1.03 | 0.93 | 1.02 | 0.97 |
| $Al_2O_3$ | 17.17 | 17.20 | 18.61 | 17.49 | 16.37 | 17.06 | 17.43 | 16.09 | 17.01 |
| FeO* | 7.92 | 7.12 | 6.59 | 7.66 | 7.87 | 6.64 | 6.22 | 6.77 | 6.49 |
| MnO | 0.14 | 0.15 | 0.10 | 0.12 | 0.15 | 0.12 | 0.13 | 0.11 | 0.12 |
| MgO | 4.02 | 3.79 | 3.86 | 4.07 | 3.14 | 4.02 | 3.25 | 3.73 | 2.97 |
| CaO | 8.49 | 7.89 | 8.21 | 7.51 | 6.82 | 6.75 | 6.43 | 6.57 | 6.37 |
| $Na_2O$ | 3.44 | 3.88 | 3.67 | 3.52 | 4.08 | 3.67 | 3.89 | 3.65 | 3.92 |
| $K_2O$ | 1.04 | 1.48 | 0.86 | 1.03 | 1.24 | 1.23 | 1.34 | 1.45 | 1.19 |
| $P_2O_5$ | 0.20 | 0.38 | 0.18 | 0.20 | 0.23 | 0.22 | 0.16 | 0.22 | 0.26 |
| Mg# | 51.6 | 52.7 | 55.1 | 52.7 | 45.6 | 55.9 | 52.3 | 53.6 | 49.0 |
| Modes (volume percent) | | | | | | | | | |
| Plagioclase | 7.7 | 20.3 | 7.6 | 22.7 | 16.9 | 22.4 | 24.7 | 25.0 | 23.2 |
| Clinopyroxene | 1.8 | 4.1 | 0.8 | 2.6 | 1.9 | 2.5 | 2.3 | 2.6 | 2.6 |
| Orthopyroxene | - | - | - | 3.0 | 1.5 | 3.2 | 3.3 | 3.5 | 5.5 |
| Olivine | 0.9 | 1.1 | - | 0.7 | - | 0.7 | 0.5 | 0.4 | 0.1 |
| Fe-Ti Oxide | - | 0.4 | - | 0.3 | 0.1 | 0.2 | 0.5 | 0.2 | 0.9 |
| Hornblende | - | - | - | - | - | - | - | - | - |
| Quartz | - | - | - | - | - | - | - | - | - |
| K-feldspar | - | - | - | - | - | - | - | - | - |
| Other | - | - | - | - | - | - | - | - | - |
| Groundmass | 89.6 | 74.1 | 91.6 | 70.7 | 79.6 | 71.0 | 68.7 | 68.3 | 67.7 |
| No. points counted | 815 | 800 | 800 | 810 | 785 | 812 | 780 | 775 | 794 |
| Texture (rock/ groundmass) | seriate/ trachytic | seriate/ intergranular | seriate/ trachytic | seriate/ intergranular | porphyritic/ pilotaxitic | porphyritic/ pilotaxitic | porphyritic/ hyalopilitic | porphyritic/ intergranular | porphyritic/ pilotaxitic |
| Trace element analyses (ppm) | | | | | | | | | |
| Ba | 193 | 422 | 184 | 192 | 222 | 226 | 241 | 264 | 250 |
| Rb | 17 | 28 | 20 | 20 | 23 | 21 | 23 | 26 | 23 |
| Sr | 390 | 545 | 432 | 375 | 308 | 401 | 377 | 311 | 329 |
| Y | 24 | 30 | 13 | 24 | 29 | 24 | 22 | 30 | 27 |
| Zr | 141 | 230 | 113 | 169 | 179 | 182 | 188 | 232 | 219 |
| Nb | 9.4 | 14.9 | 11 | 11.0 | 12.3 | 10 | 13 | 15.4 | 13 |
| Ni | 11 | 18 | 12 | 38 | 5 | 51 | 21 | 37 | 19 |
| Cu | 100 | 86 | 72 | 124 | 112 | 69 | 80 | 51 | 77 |
| Zn | 77 | 82 | 71 | 73 | 75 | 69 | 68 | 74 | 70 |
| Cr | 37 | 34 | --- | --- | 19 | --- | --- | 79 | --- |

† Sample from megablock in caldera fill.

**Table 1.** Chemical analyses of volcanic and intrusive rocks, Ariel 7.5' quadrangle—Continued

| Map No. | 37 | 38 | 39 | 40 | 41 | 42 | 43 | 44 | 45 |
|---|---|---|---|---|---|---|---|---|---|
| Field sample No. | 99LC-Q396* | 00LC-Q410s* | 00LC-Q417* | 97LC-Q122 | 00LC-Q460A* | 99LC-Q375* | 98LC-Q225 | 99LC-Q363* | 97LC-Q119 |
| Latitude (N)<br>Longitude (W) | 45°55.44'<br>122°33.60' | 45°55.86'<br>122°34.74' | 45°56.52'<br>122°33.78' | 45°59.46'<br>122°35.46' | 45°57.30'<br>122°33.30' | 45°55.26'<br>122°34.44' | 45°59.52'<br>122°33.84' | 45°56.40'<br>122°36.48' | 45°59.70'<br>122°35.82' |
| Map unit | Tdpo | Td | Td | Tdpc | Tdm | Trb | Tgb | Tgb | Tgb |
| Rock type | Dacitic welded tuff | Dacite | Dacite | Dacitic welded tuff | Dacite | Hypersthene rhyolite | Gabbro | Microgabbro | Microgabbro |
| Analyses as reported (wt. percent) | | | | | | | | | |
| $SiO_2$ | 64.73 | 66.68 | 67.62 | 64.28 | 70.29 | 70.39 | 49.39 | 51.13 | 50.43 |
| $TiO_2$ | 0.79 | 0.78 | 0.71 | 0.60 | 0.56 | 0.55 | 1.14 | 0.96 | 1.20 |
| $Al_2O_3$ | 15.07 | 15.46 | 15.31 | 13.92 | 14.90 | 15.11 | 15.94 | 19.39 | 17.37 |
| $Fe_2O_3$ | --- | --- | --- | 4.13 | --- | --- | 10.00 | --- | 8.58 |
| FeO | 5.24 | 4.65 | 4.20 | --- | 3.86 | 3.49 | --- | 7.90 | --- |
| MnO | 0.14 | 0.10 | 0.08 | 0.09 | 0.08 | 0.07 | 0.15 | 0.14 | 0.13 |
| MgO | 1.46 | 1.52 | 1.21 | 0.82 | 0.64 | 0.58 | 9.27 | 5.41 | 6.99 |
| CaO | 3.86 | 3.88 | 3.34 | 2.91 | 2.32 | 1.48 | 8.81 | 10.81 | 10.03 |
| $Na_2O$ | 4.25 | 4.55 | 4.85 | 4.20 | 4.95 | 4.26 | 2.60 | 2.60 | 2.63 |
| $K_2O$ | 1.55 | 1.96 | 2.07 | 2.10 | 2.41 | 2.89 | 0.35 | 0.64 | 0.75 |
| $P_2O_5$ | 0.20 | 0.15 | 0.15 | 0.15 | 0.13 | 0.11 | 0.24 | 0.18 | 0.26 |
| LOI | --- | --- | --- | 6.71 | --- | --- | 1.36 | --- | 1.39 |
| Total | 97.29 | 99.74 | 99.54 | 99.90 | 100.14 | 98.93 | 99.23 | 99.17 | 99.76 |
| Analyses recalculated volatile-free and normalized to 100% with all Fe as FeO (wt. percent) | | | | | | | | | |
| $SiO_2$ | 66.53 | 66.86 | 67.94 | 69.08 | 70.19 | 71.15 | 50.88 | 51.56 | 51.65 |
| $TiO_2$ | 0.81 | 0.78 | 0.71 | 0.65 | 0.56 | 0.55 | 1.18 | 0.97 | 1.23 |
| $Al_2O_3$ | 15.49 | 15.50 | 15.38 | 14.96 | 14.88 | 15.27 | 16.42 | 19.55 | 17.79 |
| FeO* | 5.39 | 4.66 | 4.22 | 4.28 | 3.85 | 3.53 | 9.47 | 7.97 | 8.04 |
| MnO | 0.15 | 0.10 | 0.08 | 0.10 | 0.08 | 0.07 | 0.15 | 0.14 | 0.13 |
| MgO | 1.50 | 1.52 | 1.22 | 0.88 | 0.64 | 0.59 | 9.55 | 5.46 | 7.16 |
| CaO | 3.97 | 3.89 | 3.36 | 3.12 | 2.32 | 1.50 | 9.08 | 10.90 | 10.27 |
| $Na_2O$ | 4.37 | 4.56 | 4.87 | 4.51 | 4.94 | 4.31 | 2.67 | 2.62 | 2.69 |
| $K_2O$ | 1.59 | 1.97 | 2.08 | 2.26 | 2.41 | 2.92 | 0.36 | 0.65 | 0.77 |
| $P_2O_5$ | 0.20 | 0.15 | 0.15 | 0.16 | 0.13 | 0.11 | 0.25 | 0.19 | 0.27 |
| Mg# | 36.9 | 40.7 | 37.7 | 30.1 | 25.8 | 25.8 | 67.9 | 58.9 | 65.1 |
| Modes (volume percent) | | | | | | | | | |
| Plagioclase | 10.2 | 19.1 | 24.0 | 10.2 | 10.0 | 13.0 | 61.9 | 64.6 | 61.3 |
| Clinopyroxene | 0.5 | 1.4 | 0.9 | 0.5 | - | - | 12.5 | 26.9 | 29.4 |
| Orthopyroxene | 0.6 | 1.8 | 1.7 | 0.5 | 0.8 | 1.8 | 11.1 | - | - |
| Olivine | - | - | - | - | - | - | 6.5 | 1.5 | 4.0 |
| Fe-Ti Oxide | 0.3 | 0.6 | 0.4 | 0.2 | 0.5 | 0.6 | 2.1 | 1.4 | 1.9 |
| Hornblende | - | - | - | - | - | - | - | - | - |
| Quartz | - | - | - | - | - | - | - | - | - |
| K-feldspar | - | - | - | - | - | - | - | - | - |
| Other | lithics: 1.0 | xenoliths: 2.4 | xenoliths: 2.9 | xenoliths: 1.3 | - | - | 5.9 | interstit. clay: 5.6 | interstit. clay:3.4 |
| Groundmass | 88.4 | 77.1 | 73.0 | 88.6 | 88.7 | 84.6 | - | - | - |
| No. points counted | 788 | 791 | 759 | 745 | 800 | 800 | 814 | 740 | 626 |
| Texture (rock/ groundmass) | porphyritic/ eutaxitic | porphyritic/ pilotaxitic | porphyritic/ pilotaxitic | porphyritic/ eutaxitic | porphyritic/ spherulitic | porphyritic/ pilotaxitic | hypidiomorphic/ granular | seriate/ intergranular | seriate/ intergranular |
| Trace element analyses (ppm) | | | | | | | | | |
| Ba | 431 | 409 | 369 | 469 | 431 | 460 | 124 | 200 | 149 |
| Rb | 49 | 41 | 39 | 85 | 51 | 73 | 5 | 9 | 14 |
| Sr | 415 | 260 | 224 | 191 | 185 | 99 | 355 | 621 | 482 |
| Y | 48 | 35 | 35 | 36 | 37 | 89 | 15 | 18 | 17 |
| Zr | 336 | 262 | 284 | 318 | 345 | 422 | 75 | 108 | 131 |
| Nb | 19.5 | 13.3 | 15.3 | 18 | 18.9 | 21 | 9 | 7 | <10 |
| Ni | 9 | 5 | 5 | --- | 5 | 7 | 192 | 21 | --- |
| Cu | 41 | 33 | 40 | --- | 20 | 25 | 91 | 62 | --- |
| Zn | 80 | 61 | 52 | --- | 55 | 54 | 83 | 69 | --- |
| Cr | 0 | 5 | 0 | --- | 0 | 0 | --- | 62 | --- |

**Table 1.** Chemical analyses of volcanic and intrusive rocks, Ariel 7.5' quadrangle—Continued

| Map No. | 46 | 47 | 48 | 49 | 50 | 51 | 52 | 53 | 54 |
|---|---|---|---|---|---|---|---|---|---|
| Field sample No. | 98LC-Q255 | 98LC-Q184B | 99LC-Q323A | 98LC-Q185A | 98LC-Q175 | 98LC-Q171 | 98LC-Q190 | 99LC-Q346A* | 99LC-Q386* |
| Latitude (N)<br>Longitude (W) | 45°58.38'<br>122°32.88' | 45°58.32'<br>122°33.36' | 45°57.54'<br>122°35.94' | 45°58.38'<br>122°33.12' | 45°54.00'<br>122°30.36' | 45°56.28'<br>122°34.92' | 45°54.96'<br>122°35.16' | 45°58.56'<br>122°36.96' | 45°55.50'<br>122°35.58' |
| Map unit | Tgb | Tdi | Tiba | Tdi | Tiba | Tdi | Tdi | Tdi | Tqd |
| Rock type | Gabbro | Diorite | Basaltic andesite | Diorite | Basaltic andesite | Microdiorite | Microdiorite | Microdiorite | Micro-quartz diorite |
| Analyses as reported (wt. percent) | | | | | | | | | |
| $SiO_2$ | 51.14 | 50.62 | 52.75 | 52.94 | 53.42 | 53.80 | 53.63 | 55.05 | 57.38 |
| $TiO_2$ | 1.07 | 1.14 | 0.89 | 1.14 | 1.33 | 0.94 | 0.97 | 0.79 | 1.24 |
| $Al_2O_3$ | 17.06 | 17.38 | 18.81 | 17.21 | 16.04 | 17.54 | 17.73 | 19.69 | 17.65 |
| $Fe_2O_3$ | 9.19 | 9.64 | --- | 8.78 | 9.94 | 8.09 | 7.80 | --- | --- |
| FeO | --- | --- | 7.49 | --- | --- | --- | --- | 6.82 | 8.12 |
| MnO | 0.14 | 0.15 | 0.13 | 0.14 | 0.17 | 0.14 | 0.16 | 0.11 | 0.16 |
| MgO | 7.45 | 5.21 | 5.81 | 4.62 | 4.69 | 5.19 | 5.16 | 4.35 | 2.35 |
| CaO | 9.24 | 8.20 | 9.96 | 8.86 | 9.01 | 8.69 | 8.80 | 9.13 | 7.36 |
| $Na_2O$ | 2.73 | 3.41 | 2.70 | 3.15 | 3.11 | 2.99 | 3.09 | 3.15 | 4.08 |
| $K_2O$ | 0.53 | 1.07 | 0.92 | 0.75 | 0.41 | 0.74 | 0.71 | 0.47 | 0.85 |
| $P_2O_5$ | 0.17 | 0.16 | 0.16 | 0.19 | 0.22 | 0.15 | 0.16 | 0.14 | 0.19 |
| LOI | 0.88 | 2.60 | --- | 1.73 | 1.29 | 1.44 | 1.45 | --- | --- |
| Total | 99.58 | 99.59 | 99.63 | 99.50 | 99.62 | 99.71 | 99.65 | 99.70 | 99.39 |
| Analyses recalculated volatile-free and normalized to 100% with all Fe as FeO (wt. percent) | | | | | | | | | |
| $SiO_2$ | 52.25 | 52.57 | 52.95 | 54.53 | 54.80 | 55.13 | 54.98 | 55.22 | 57.73 |
| $TiO_2$ | 1.09 | 1.18 | 0.89 | 1.17 | 1.36 | 0.96 | 0.99 | 0.79 | 1.25 |
| $Al_2O_3$ | 17.42 | 18.05 | 18.88 | 17.73 | 16.45 | 17.97 | 18.17 | 19.75 | 17.76 |
| FeO* | 8.56 | 9.29 | 7.52 | 8.32 | 9.33 | 7.59 | 7.33 | 6.84 | 8.17 |
| MnO | 0.14 | 0.16 | 0.13 | 0.14 | 0.17 | 0.14 | 0.17 | 0.11 | 0.16 |
| MgO | 7.61 | 5.41 | 5.83 | 4.76 | 4.81 | 5.32 | 5.29 | 4.36 | 2.36 |
| CaO | 9.44 | 8.52 | 10.00 | 9.13 | 9.24 | 8.90 | 9.02 | 9.16 | 7.41 |
| $Na_2O$ | 2.79 | 3.54 | 2.71 | 3.24 | 3.19 | 3.07 | 3.16 | 3.16 | 4.11 |
| $K_2O$ | 0.54 | 1.11 | 0.92 | 0.78 | 0.42 | 0.76 | 0.73 | 0.47 | 0.86 |
| $P_2O_5$ | 0.18 | 0.17 | 0.16 | 0.2 | 0.22 | 0.15 | 0.16 | 0.14 | 0.20 |
| Mg# | 65.1 | 55.0 | 61.9 | 54.6 | 52.0 | 59.5 | 60.2 | 57.2 | 37.8 |
| Modes (volume percent) | | | | | | | | | |
| Plagioclase | 59.3 | 66.2 | 22.5 | 64.7 | 0.3 | 20.8 | 19.5 | 65.7 | 19.8 |
| Clinopyroxene | 12.0 | 16.8 | 3.3 | 13.1 | 0.2 | 6.4 | - | 5.3 | 0.1 |
| Orthopyroxene | 14.0 | 9.0 | - | 7.5 | - | - | - | 10.6 | - |
| Olivine | 5.6 | - | 5.5 | 3.5 | 0.2 | 4.6 | 4.3 | 0.4 | - |
| Fe-Ti Oxide | 1.8 | 1.8 | - | 0.4 | - | 0.1 | - | 1.6 | 0.1 |
| Hornblende | - | - | - | - | - | - | - | - | - |
| Quartz | 1.3 | - | - | 5.8 | - | - | - | 1.8 | - |
| K-feldspar | granophyre: 1.2 | - | - | granophyre: 5.0 | - | - | - | - | - |
| Other | 4.8 | 6.2 | - | - | - | - | - | - | - |
| Groundmass | - | - | 68.7 | - | 99.3 | 68.1 | 76.2 | 14.6 | 80.0 |
| No. points counted | 850 | 777 | 787 | 810 | 750 | 792 | 814 | 813 | 810 |
| Texture (rock/ groundmass) | hypidiomorphic/ granular | hypidiomorphic/ granular | seriate/ intergranular | hypidiomorphic/ granular | sparsely phyric/ trachytic | seriate/ intergranular | seriate/ intergranular | seriate/ intergranular | seriate/ intergranular |
| Trace element analyses (ppm) | | | | | | | | | |
| Ba | 173 | 251 | 152 | 166 | 163 | 169 | 137 | 117 | 191 |
| Rb | 11 | 28 | 10 | 16 | 10 | 13 | 15 | 5 | 25 |
| Sr | 343 | 427 | 505 | 338 | 319 | 332 | 334 | 446 | 366 |
| Y | 18 | 16 | 16 | 21 | 25 | 16 | 24 | 17 | 29 |
| Zr | 107 | 99 | 100 | 114 | 132 | 104 | 116 | 112 | 123 |
| Nb | 10 | 7 | 5.3 | 12 | 10 | 12 | 8.0 | 6.1 | 8.5 |
| Ni | 124 | 36 | 45 | 31 | 14 | 58 | 80 | 36 | 2 |
| Cu | 117 | 207 | 58 | 150 | 167 | 119 | 54 | 345 | 103 |
| Zn | 71 | 82 | 64 | 70 | 88 | 72 | 69 | 72 | 89 |
| Cr | --- | --- | 80 | --- | --- | --- | --- | 38 | 6 |

**Table 1.** Chemical analyses of volcanic and intrusive rocks, Ariel 7.5' quadrangle—Continued

| Map No. | 55 | 56 | 57 | 58 | 59 | 59 | 60 | 60 | 60 |
|---|---|---|---|---|---|---|---|---|---|
| Field sample No. | 99LC-Q335* | 97LC-Q138 | 97LC-Q121B | 98LC-Q288A† | SC02-539A‡ | SC02-539B‡ | 00LC-Q461 | SC02-538A‡ | SC02-538B‡ |
| Latitude (N) | 45°58.68' | 45°59.34' | 45°59.70' | 45°59.04' | 45°59.16 | 45°59.16' | 45°57.18' | 45°57.18' | 45°57.18' |
| Longitude (W) | 122°36.48' | 122°35.10' | 122°35.52' | 122°31.56' | 122°33.49' | 122°33.49' | 122°33.48' | 122°33.48' | 122°33.48' |
| Map unit | Tqd | Tid | Tid | Qbh | Qat | Qat | Qssw | Qssw | Qssw |
| Rock type | Micro-quartz diorite | Dacite | Dacite | Basalt clasts in hyaloclastite | Dacite boulder in till | Dacite boulder in till | Dacite boulder in lahar | Dacite boulder in lahar | Dacite boulder in lahar |
| Analyses as reported (wt. percent) | | | | | | | | | |
| $SiO_2$ | 60.00 | 62.21 | 63.24 | 50.45 | 63.10 | 64.40 | 63.56 | 63.30 | 64.00 |
| $TiO_2$ | 0.85 | 1.13 | 1.05 | 1.64 | 0.54 | 0.58 | 0.62 | 0.62 | 0.68 |
| $Al_2O_3$ | 17.64 | 15.07 | 14.94 | 16.39 | 18.20 | 17.60 | 17.23 | 17.20 | 17.40 |
| $Fe_2O_3$ | --- | 6.78 | 6.45 | --- | 3.95 | 4.09 | --- | 4.44 | 4.70 |
| FeO | 5.61 | --- | --- | 10.77 | --- | --- | 4.07 | --- | --- |
| MnO | 0.10 | 0.13 | 0.13 | 0.19 | 0.07 | 0.08 | 0.07 | 0.07 | 0.08 |
| MgO | 3.20 | 1.60 | 1.41 | 6.11 | 1.51 | 1.31 | 2.07 | 2.01 | 1.89 |
| CaO | 6.79 | 4.45 | 4.01 | 9.45 | 4.05 | 3.42 | 5.01 | 4.89 | 4.91 |
| $Na_2O$ | 3.90 | 5.12 | 4.97 | 3.68 | 4.48 | 3.88 | 4.60 | 4.38 | 4.50 |
| $K_2O$ | 1.23 | 0.71 | 1.20 | 0.51 | 1.21 | 1.53 | 1.43 | 1.36 | 1.32 |
| $P_2O_5$ | 0.18 | 0.31 | 0.31 | --- | 0.11 | 0.12 | 0.15 | 0.14 | 0.15 |
| LOI | --- | 2.40 | 1.60 | --- | 3.04 | 2.94 | --- | 1.61 | 0.74 |
| Total | 99.49 | 99.91 | 99.31 | 99.19 | 100.26 | 99.95 | 98.80 | 100.02 | 100.37 |
| Analyses recalculated volatile-free and normalized to 100% with all Fe as FeO (wt. percent) | | | | | | | | | |
| $SiO_2$ | 60.31 | 64.14 | 65.06 | 50.86 | 0.56 | 0.60 | 64.33 | 64.57 | 64.53 |
| $TiO_2$ | 0.85 | 1.16 | 1.08 | 1.65 | 18.78 | 18.20 | 0.62 | 0.63 | 0.69 |
| $Al_2O_3$ | 17.73 | 15.54 | 15.37 | 16.52 | 3.77 | 3.92 | 17.44 | 17.55 | 17.54 |
| FeO* | 5.64 | 6.45 | 6.11 | 10.86 | 0.07 | 0.08 | 4.12 | 4.14 | 4.28 |
| MnO | 0.10 | 0.14 | 0.14 | 0.19 | 1.56 | 1.35 | 0.07 | 0.07 | 0.08 |
| MgO | 3.22 | 1.65 | 1.45 | 6.16 | 4.18 | 3.54 | 2.10 | 2.05 | 1.91 |
| CaO | 6.82 | 4.59 | 4.12 | 9.53 | 4.62 | 4.01 | 5.07 | 4.99 | 4.95 |
| $Na_2O$ | 3.92 | 5.28 | 5.12 | 3.71 | 1.25 | 1.58 | 4.66 | 4.47 | 4.54 |
| $K_2O$ | 1.24 | 0.74 | 1.23 | 0.51 | 0.11 | 0.12 | 1.45 | 1.39 | 1.33 |
| $P_2O_5$ | 0.18 | 0.32 | 0.32 | --- | 0.56 | 0.60 | 0.15 | 0.14 | 0.15 |
| Mg# | 54.5 | 35.0 | 33.2 | 54.3 | 46.4 | 42.0 | 51.6 | 50.9 | 48.3 |
| Modes (volume percent) | | | | | | | | | |
| Plagioclase | 22.9 | 7.8 | 2.8 | --- | --- | --- | 35.1 | --- | --- |
| Clinopyroxene | 3.4 | 0.7 | 0.2 | --- | --- | --- | | --- | --- |
| Orthopyroxene | 2.4 | 1.0 | 0.1 | --- | --- | --- | 3.1 | --- | --- |
| Olivine | 0.9 | - | - | --- | --- | --- | | --- | --- |
| Fe-Ti Oxide | 0.2 | 0.5 | 0.1 | --- | --- | --- | 1.5 | --- | --- |
| Hornblende | - | - | - | --- | --- | --- | 5.1 | --- | --- |
| Quartz | - | - | - | --- | --- | --- | | --- | --- |
| K-feldspar | - | - | - | --- | --- | --- | | --- | --- |
| Other | - | - | - | --- | --- | --- | | --- | --- |
| Groundmass | 70.2 | 90.0 | 96.8 | --- | --- | --- | 55.2 | --- | --- |
| No. points counted | 800 | 602 | 783 | --- | --- | --- | 800 | --- | --- |
| Texture (rock/ groundmass) | seriate/ intergranular | porphyritic/ pilotaxitic | sparsely phyric/ pilotaxitic | porphyritic/ vitric | porphyritic/ felsitic | porphyritic/ felsitic | porphyritic/ felsitic | porphyritic/ felsitic | porphyritic/ felsitic |
| Trace element analyses (ppm) | | | | | | | | | |
| Ba | 205 | 326 | 315 | --- | --- | --- | 295 | --- | --- |
| Rb | 14 | 48 | 38 | --- | --- | --- | 30 | --- | --- |
| Sr | 470 | 283 | 249 | --- | --- | --- | 587 | --- | --- |
| Y | 20 | 30 | 32 | --- | --- | --- | 11 | --- | --- |
| Zr | 164 | 255 | 258 | --- | --- | --- | 114 | --- | --- |
| Nb | 9.4 | 13 | 19 | --- | --- | --- | 6.0 | --- | --- |
| Ni | 23 | --- | ND | --- | --- | --- | 15 | --- | --- |
| Cu | 121 | --- | 53 | --- | --- | --- | 11 | --- | --- |
| Zn | 64 | --- | 92 | --- | --- | --- | 56 | --- | --- |
| Cr | 20 | --- | --- | --- | --- | --- | 13 | --- | --- |

† Average of 21 spot analyses by electron microprobe at U.S. Geological Survey, Menlo Park, Calif.; J.P. Walker, analyst.
‡ Data provided by M.A. Clynne, U.S. Geological Survey, written commun., 2003.

**Table 2.** Summary of $^{40}Ar/^{39}Ar$ incremental-heating age determinations, Ariel 7.5' quadrangle

| Field sample no. | Location | | Map unit | Rock type | Material dated | Age (±1σ error) | Source |
|---|---|---|---|---|---|---|---|
| | Latitude (N) | Longitude (W) | | | | | |
| 98LC-Q219B | 45°59.16' | 122°33.48' | Qso | Pumice-lapilli bed | Plagioclase | 269±13 ka | R.J. Fleck, written commun., 2003 |
| 99LC-Q396 | 45°55.44' | 122°33.60' | Tdpo | Dacitic welded tuff | Plagioclase | 35.1±0.3 Ma | R.J. Fleck, written commun., 2001 |
| 97LC-Q122 | 45°59.46' | 122°35.46' | Tdpc | Dacitic welded tuff | Plagioclase | 35.2±0.3 Ma | R.J. Fleck, written commun., 1999 |